Effect of Strain on Structure and Morphology of Ultrathin Ge Films on Si(001)

Feng Liu, Fang Wu, and M. G. Lagally*

University of Wisconsin—Madison, Madison, Wisconsin 53706

Received February 26, 1997 (Revised Manuscript Received April 17, 1997)

Contents

I. Introduction

Conventional surface probes are usually diffraction-based techniques, by which real-space surface structures are indirectly derived from their representations in the reciprocal space. While diffraction probes are very useful in determining the long-range order of a surface, they often suffer from ambiguities in atomic details. The advance of a new generation of surface probes based on *force and tunneling microscopy* has allowed the direct observation of surfaces in real space, with atomic resolution. The applications of these new techniques continue to develop and expand seemingly without limits, from probing surface atomic, electronic, and optical properties to determining quantitatively surface thermodynamics and growth kinetics and to patterning surfaces at the nanometer scale. Scanning tunneling microscopy (STM) is one of the most widely used probes of the new generation. In this article, we review recent applications of STM, as a quantitative tool for studying surface structures, morphologies, energetics, and stresses, to investigating the effect of strain during the growth of ultrathin Ge films on Si(001).

The potential of creating novel electronic and optoelectronic devices from SiGe/Si heterojunctions and nanostructures has recently generated considerable excitement.[1] Epitaxial growth of Ge and SiGe alloy on Si is also a classical model system for investigating the effect of misfit strain on heteroepitaxy. Understanding the morphological instabilities, such as surface roughening processes, in a strained film is very important to the growth of high-quality smooth films beyond the "equilibrium critical thickness" [2,3] by manipulating the growth kinetics and modifying the surface thermodynamics.[4] Furthermore, recent efforts have also been made to take advantage of certain surface roughening processes that have been recognized as useful means for nanofabrication by strain-induced self-assembly and self-organization of steps and clusters.[5]

Thin-film growth is controlled by the competition between kinetics of growth and the thermodynamics of the thin film/substrate system. Usually, at low temperature and/or high deposition rate, growth is dominated by kinetics: at those conditions there exists a large supersaturation of adsorbed atoms, the system is far from equilibrium; at high temperature and/or low deposition rate, the thermodynamic conditions become more apparent. STM can be used to investigate both the growth kinetics and the thin-film thermodynamics with atomic resolution. For example, STM has determined[6] the adatom diffusion coefficient and kinetics of interaction between adatoms and surface steps through the measurement of island number density and the measurement of the denuded zone width near surface steps, during homoepitaxial growth of Si on Si(001) in the submonolayer regime.

Similar studies have also been made for heteroepitaxial growth of Ge on Si(001),[7,8] which will be discussed briefly later. However, the main body of this review will be on quantitative STM determinations of thermodynamic properties of thin Ge films grown on Si(001), including quasi-equilibrium surface structures and morphologies, energetics of defects and of defect−defect interactions, and evolving surface stress tensors. The purpose of the review is to reveal the strain-induced surface roughening and ordering processes during the initial stage of growth of pure Ge on Si(001), focusing on quantitative STM analyses of evolving surface structures, morphologies, and stress tensors. We attempt to present a comprehensive picture of thermodynamics of a strained ultrathin Ge film [up to a thickness of a few monolayers (MLs)] on Si(001), revealing the physical mechanisms of strain relaxation and understanding the intriguing interplay between surface stress and surface morphology.

S0009-2665(96)00072-6 CCC: $28.00

Feng Liu is currently an Associate Research Scientist in the Department of Materials Science and Engineering at the University of Wisconsin—Madison. He was a postdoctoral research associate at Rutgers University from 1991 to 1993 and at Oak Ridge National Lab from 1993 to 1995. He graduated with his Ph.D. in Chemical Physics from Virginia Commonwealth University in 1990, receiving the Academic Excellent Graduate Award. He is a member of the Materials Research Society and the American Physical Society. He is also a life member of the Sigma Pi Sigma Physics Honor Society and the Phi Kappa Phi Science Honor Society. He was appointed as a guest professor at Tianjin Normal University, China, in 1995. His research interests lie in the development and application of first-principles and empirical theoretical methods to study structural and electronic properties of solid materials, and, more recently, in the modeling and simulation of surfaces, thin-film growth, and nanofabrication. He has published over 30 papers in these areas.

Fang Wu is currently a Project Engineer in the R&D Department at Komag Incorporated, the world's largest independent thin-film magnetic recording media supplier for information storage. He graduated with his Ph.D. in Materials Science from University of Wisconsin—Madison in 1995. He is a member of the Materials Research Society. His Ph.D. research focused on the quantitative study of semiconductor surface structures and initial stage thin-film growth mechanism using scanning tunneling microscopy and computer simulation, on which he has published 10 research papers. His recent activities at Komag include developing a new advanced overcoat for the disk media and new storage technology.

Max G. Lagally is Erwin W. Mueller Professor of Materials Science and Engineering and of Physics at the University of Wiisconsin—Madison. He received his Ph.D. in physics from the University of Wisconsin in 1968, and after a postdoctoral fellowship at the Fritz-Haber Institute of the Max Planck Society in Berlin, Germany, returned to Madison to join the Department of Materials Science and Engineering in 1971. He is a registered engineer in the State of Wisconsin. In 1990 he was appointed to a concurrent position as professor in the Physics Department. His research has focused on identifying the relationship of structure and morphology of surfaces and thin films to their chemical and physical properties, in identifying and quantifying the atomistic mechanisms of film growth, and, more recently, in using controlled surface and thin-film morphologies to create structures with novel properties. He is a Fellow of the American Physical Society, the American Vacuum Society, and the Australian Institute of Physics. He received the highest award of the American Vacuum Society, the Medard W. Welch Award in 1991, the David Adler Lectureship Award of the American Physical Society in 1994, the MRS Medal of the Materials Research Society in 1994, and the Davisson-Germer Prize of the American Physical Society in 1995. He has held visiting appointments (in 1987) in Sydney, Australia, as the Gordon Godfrey Visiting Professor of Physics at the University of New South Wales, and (in 1992-1993) in Jülich, Germany, as a Humboldt Senior Research Fellow. He has also held an Alfred P. Sloan Foundation Fellowship. He has been on the editorial boards of the *Journal of Vacuum Science and Technology* (1978-1981) and the *Journal of Materials Research* (as a principal editor, 1990-1993) and serves on the editorial boards of *Surface Science* (1994 to present) and of *The Review of Scientific Instruments* (1997 to present). His service to professional societies has been extensive. He is presently a member of the Board of Trustees of the American Vacuum Society, the Executive Committee of the Materials Physics Division of the American Physical Society, and the Awards Committee of the Materials Research Society. He has published over 250 papers on metal and semiconductor surface science, on film growth, and on the development of instrumentation and analytical methods for the analysis of the properties of surfaces and thin films. He has edited or coedited three books, *Methods of Experimental Physics: Surfaces*, *Kinetics of Ordering and Growth at Surfaces*, and *Evolution of Surface and Thin-Film Microstructure*.

II. Intrinsic Surface Stress of Si(001) and Ge/Si(001)

The surface energy of a solid surface has in general two contributions: the formation energy and the deformation energy. The former reflects the breaking of bonds to make a solid surface; the latter reflects the tendency of a solid surface to distort because it is a quasi-2D system and hence would like to assume a different atomic structure and a bonding configuration different from that of the bulk. The deformation energy gives rise to a nonvanishing surface stress. The nonzero surface stress tensor, i.e., the consequence of this second term in the surface energy, is defined as the derivative of surface energy (E_{surf}) with respect to surface strain (ϵ_{ij})

$$\sigma_{ij} = \frac{\mathrm{d}E_{\mathrm{surf}}}{\mathrm{d}\epsilon_{ij}} \tag{1}$$

Surface stress plays an important role in many fascinating and intriguing surface phenomena that appear on Si(001). For clean Si(001), the most prominent feature is the (2×1) reconstruction[9,10] (see Figure 1). Surface atoms form rows of dimers to reduce surface "chemical" energy by removing half of the dangling bonds, but at the expense of increasing surface "strain" energy due to bond distortion. The reconstruction introduces a highly anisotropic surface stress: the stress $\sigma_{||}$ along the dimer bond is tensile (i.e., surface atoms would like to be closer

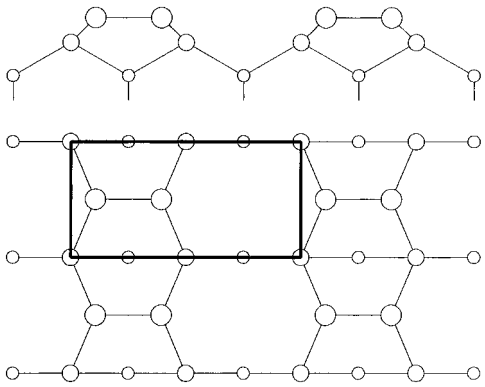

Figure 1. Side view (top panel, [110] projection) and top view (bottom panel) of the (2×1) reconstructed Si(001) surface. The dark rectangle depicts a (2×1) unit cell of dimension 7.70 Å × 3.85 Å. The dimer bond length is about 2.2 Å.

together along this direction than they are); the stress $\sigma_\perp$ along the dimer row is consequently compressive (or at least less tensile than $\sigma_{||}$). This stress anisotropy, $F = \sigma_{||} - \sigma_\perp$, is predicted to cause a morphological instability:[11,12] a single-domain surface breaks up into a stripelike structure with alternating stress domains. Such stress domains are quite generally possible in systems that lower their surface energy by reconstruction.

On a vicinal Si(001) surface, with a small miscut toward a ⟨110⟩ direction, the surface misorientation induces such a stress-domain structure, consisting of alternating (2×1) and (1×2) domains separated by monatomic steps. The discontinuity of stress at the step introduces a force monopole proportional to the stress anisotropy, giving rise to a repulsive interaction between steps. The surface strain energy is expressed as $E_s = C_1 - C_2 \ln(L/a)$,[11,12] where C_1 denotes the step formation energy per unit length, C_2 reflects the strength of the elastic step−step repulsion, L is the step−step separation (terrace width), and a is a microscopic cutoff length on the order of a lattice constant. When a uniaxial external stress is applied to such a surface, the favored domain type will grow at the expense of the other through step motion (given that there is no kinetic limitation).[12,13] A measurement[13] of the population asymmetry of (2×1) and (1×2) domains as a function of the external stress determines quantitatively the intrinsic surface stress anisotropy of Si(001) as 0.07 ± 0.02 eV/Å^2. The stress anisotropy of Si(001) has also been calculated by various theoretical methods,[14−17] and good agreement with experiment has finally been reached after several years of controversy.[16,17]

As Ge atoms are deposited onto Si(001), they stay in registry with the substrate Si atoms for several monolayers,[18] keeping the basic dimerized surface structure intact (although dimers have a stronger tendency to buckle on Ge-covered Si(001) than on clean Si(001)[19−21]). Total-energy calculations[22] that assume a (2×1) structure is maintained (i.e., without vacancy formation and (2×n) reconstruction), show that surface stress would change toward compression in both dimer-bond and dimer-row directions, reflecting the buildup of stress in the deposited film due to lattice mismatch, with the surface stress anisotropy essentially constant. In reality, however, the large compression along the dimer-row direction is relieved by the formation of dimer vacancies. The ordering of vacancies [i.e., the (2×n) reconstruction] drastically changes the intrinsic surface stress field, reversing progressively the sign of the stress anisotropy of clean Si(001) with increasing Ge coverage.[23] The stress anisotropy of a Ge/Si(001) surface becomes close to zero at 1 ML Ge coverage and −0.06 ± 0.02 eV/Å^2 at 2 ML Ge coverage.[23]

III. Submonolayer Growth

In heteroepitaxy, such as the growth of Ge on Si, the strain induced by lattice mismatch is expected to affect both kinetics and thermodynamics. At room temperature, as Ge atoms are deposited onto a Si(001) substrate, they initially form 2D epitaxial islands just as in homoepitaxy via the following steps:[6−8,24] adatom adsorption, adatom diffusion, nucleation of islands, and growth of islands. Both experiments[7,8] and theories[25−27] show that the kinetics of growth of Ge on Si(001) in the submonolayer regime is essentially the same as that of Si(001) homoepitaxy. A first-principles calculation of the potential-energy surface for a Ge adatom on Si(001) shows that[27] the most stable adsorption site for a Ge adatom is in the trough, next to a dimer row and between two dimers, as for a Si adatom.[28] STM measurements[6−8] show that the diffusion of both Si and Ge adatoms is highly anisotropic, moving along the dimer-row direction about 1000 times faster than across the dimer rows. The activation barrier for diffusion of Ge resembles that of Si on Si(001), but the prefactor is an order of magnitude smaller, implying that Ge atoms diffuse more slowly on Si(001) than do Si atoms.[8] The calculated diffusion barriers[27,28] agree well with experiments. At room temperature, for growth of both Si and Ge, the size of critical nuclei is one atom.[6−8] The as-grown 2D epitaxial islands have a highly anisotropic shape due to the large difference in sticking coefficients of adatoms to different step edges;[6−8] annealing at higher temperatures (∼600 K) changes the islands into a much more rounded shape whose aspect ratio is determined by the energetics of two types of monatomic height steps.[29]

One can conclude, therefore, that the 4.2% lattice mismatch between Ge and Si has little effect on the kinetics of submonolayer growth of Ge on Si(001). After the completion of the first Ge monolayer, however, the kinetics of further growth of Ge changes drastically. It has been shown[8] that the diffusion of Ge adatoms on one-monolayer Ge-covered Si(001) is much less anisotropic than on clean Si(001) and that overall the effective diffusion coefficient is lower. Both these changes are believed to be caused[8] by strain-induced (2×n) reconstruction (see next section), consisting of ordered dimer-vacancy lines that impose an additional barrier to diffusion along the dimer rows, as shown by theories.[26,30]

Some differences between Ge and Si on Si(001) have been observed by STM. Single Ge dimers and dimers in Ge islands (rows of dimers), although similar to their Si counterparts in overall shape, size, and kinetic behavior, have[19−21,31] a much stronger tendency to buckle on Si(001) than their Si counter-

parts. The buckling leads a single Ge dimer (or a Si−Ge mixed dimer) to undergo a rocking motion at room temperature,[31] while a unbuckled Si dimer rotates back and forth.[32−35] The different dynamic motions of a Ge dimer (or a mixed Si−Ge dimer) and a Si dimer at room temperature actually provide us a unique way to distinguish them[31] (see section VI). The adsorption of a Ge monomer[27] or a Ge dimer[31] also induces buckling of Si substrate dimer rows underneath and next to the adsorbate. These buckling effects are likely to be a manifestation of the larger size of Ge atoms.

In practice, thin-film growth is often carried out at temperatures [~600 °C for Ge on Si(001)] much higher than room temperature, using step flow to facilitate smooth growth. Thus, some aspects of growth kinetics can become more complex, e.g., those due to possible exchange of Ge and Si during adsorption (see section VI) and increase of critical nuclei size.[36] On the other hand, films grown at sufficiently high temperatures are very close to thermodynamic equilibrium. For a Ge film grown on Si(001), the quasi-equilibrium is characterized by the formation of $(2\times n)$ reconstruction; the well-ordered dimer-vacancy lines can only be obtained by either growing at a sufficiently high temperature (>300 °C) or growing at room temperature followed by annealing at a higher temperature.[37] A recent analysis shows that[38] the supersaturation is very low at such high temperatures, so the structure and morphology of the thin film is dominated by thermodynamics. In the rest of this review, we will focus mostly on quasi-equilibrium Ge films grown or annealed at typical growth temperatures (500−700 °C), paying special attention to the effect of strain on their structural and morphological evolution.

IV. Formation and Ordering of Dimer Vacancies

A. Rebonded Dimer Vacancy

Dimer vacancies and their complexes were recognized as intrinsic surface defects on Si(001) since Si(001) was first imaged with STM.[10] The single-dimer vacancy can have either a non-rebonded, metastable configuration or a rebonded, stable configuration. The rebonding of the exposed second-layer atoms, similar to the dimerization of surface atoms, reduces the number of dangling bonds at the expense of introducing a tensile stress along the bonding direction (i.e., the dimer-row direction).[39,40] First-principles calculations[41,42] show that the formation energy for a rebonded single-dimer vacancy on Si(001) can be as low as ~0.2−0.3 eV/dimer. Measurements[42,43] of the electronic structure of a single-dimer vacancy indirectly confirm the rebonded configuration.

When a lattice mismatched film such as Ge is deposited onto Si(001), misfit strain is expected to be relieved, given sufficient kinetics, by roughening of the growth front, which may appear in various different forms, such as creation of defects (vacancies, steps, etc.), modulation of the surface through the formation and/or rearrangement of steps, and growth of 3D coherent islands. At what stage a process is initiated depends on the formation energy of the induced structure or morphology by each process and on kinetic limitations. One process can preempt or initiate another.

When Ge is added to the surface, the stress state of the surface is modified. Initial strain relaxation of the overlayer is primarily achieved by forming additional dimer vacancies. Total-energy calculations[22,30,40] show that dimer vacancies actually have a *negative* formation energy on the Ge/Si(001) surface with respect to the uniformly strained Ge overlayer, and hence they are energetically even more favored to form in a Ge layer on Si(001) than on clean Si(001). Although the kinetics of vacancy formation are not known, we should expect that dimer vacancies are also kinetically more favored to form on Ge/Si(001) than on clean Si(001), because it is easier to break Si−Ge or Ge−Ge bonds than to break Si−Si bonds.

The rebonding of second-layer atoms in the dimer vacancies plays an important role in the mechanisms of vacancy formation and strain relaxation in Ge-covered Si(001). Vacancies can serve as a strain−relief mechanism by simply providing room for the expansion of the Ge overlayer. Without rebonding, however, vacancy formation would cost too much chemical energy through the creation of dangling bonds. The rebonding of second-layer atoms in the vacancies not only eliminates the dangling bonds but also introduces a large tensile stress, which cancels and even over-compensates the large compression along the dimer rows in the Ge overlayer.[22,40] Thus, vacancy formation is driven both by the reduction in the number of dangling bonds and by strain relaxation.

B. $(2\times n)$ Reconstruction and Vacancy−Vacancy Interaction

The ordering of vacancies to form the $(2\times n)$ reconstruction will further reduce the surface strain energy. As the Ge coverage increases, more and more dimer vacancies (DVs) form. At high enough vacancy concentration, the DV−DV interaction drives DVs on different dimer rows to order in the direction perpendicular to the dimer rows, forming vacancy lines (VLs). On average, two adjacent VLs are separated by na_0, leading to the $(2\times n)$ reconstruction; a_0 here is the surface lattice constant. The reconstruction has been observed on Ge-covered Si(001) by both STM[7,44,45] and LEED,[44,45] and has also been seen during the deposition of SiGe alloy on Si(001) because of Ge surface segregation.[46,47] Recent quantitative STM studies[23,48−50] have helped to unravel the physical origin of the $(2\times n)$ reconstruction[48] and to reveal its complex effect on step morphology[49] and surface stress field.[23]

Although dimer vacancies readily form on clean Si(001), a well-defined $(2\times n)$ pattern begins to appear only beyond 0.8 ML Ge coverage (θ_{Ge}),[49,50] suggesting that the reconstruction, (i.e., the ordering of vacancies) is related to relief of misfit-induced compressive strain in the surface.[40,44] This conclusion is supported by an STM observation[7] that at the tops of large 3D Ge islands, where the strain is relaxed, flat (001) facets show only a perfect (2×1) reconstruction. Figure 2 shows an STM image of a $(2\times n)$ structure on a Ge-covered Si(001) surface with $\theta_{Ge} \approx 1.6$ ML,

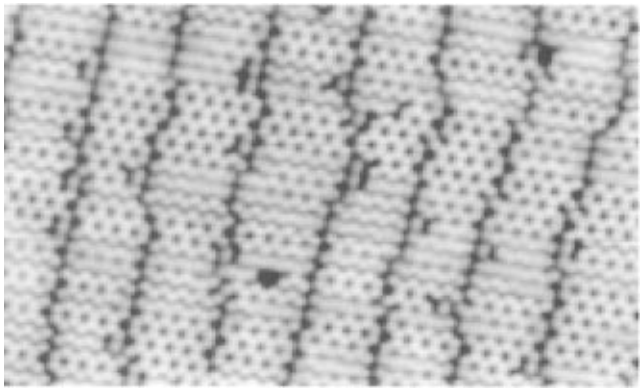

Figure 2. STM image of the Ge-covered Si(001) surface showing the $(2\times n)$ reconstruction. Size of the image is ~300 Å × 200 Å. (Courtesy of X. R. Qin.)

where the VLs are visible as dark lines because of the lower altitudes of the dimer-vacancy sites. The $(2\times n)$ reconstruction is not perfect; each DV fluctuates around its mean position. The meandering of the VLs is dictated by the competition between the ordering process, driven by the DV−DV interaction to minimize elastic energy, and the disordering process, driven by a desire of the system to maximize its configurational entropy.

1. Distribution of Dimer Vacancies

By analyzing the thermal fluctuations around the ideal $(2\times n)$ structure, the form as well as the magnitude of the DV−DV interaction has been determined.[48] Figure 3, a schematic diagram of the $(2\times n)$ structure, introduces the notation for DV displacements to facilitate discussion of their distribution and of subsequent analyses. As discussed in section IV.A, the rebonding of the second-layer atoms in a DV pulls these atoms together along the dimer row direction, giving rise to a large tensile stress in this direction. (The rebonding does not induce any long-range elastic field in the perpendicular direction.[22,40]) The tensile stress due to second-layer rebonding effectively cancels the compressive stress due to Ge/Si lattice mismatch, thus lowering the elastic energy. There exists a preferred spacing na_0 between two neighboring DVs on the same dimer row. When they are too far apart, the compressive

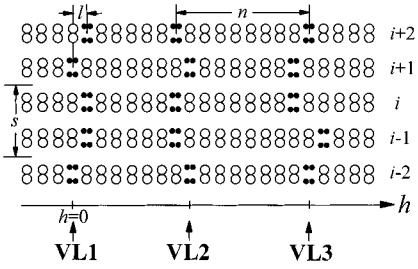

Figure 3. Schematic diagram showing the atomic structure of the $(2\times n)$ reconstruction. The open and solid circles represent the top- and second-layer atoms, respectively. Two connected atoms form a dimer, and the dimers align into dimer rows labeled by i, $i \pm 1$, etc. Within each dimer vacancy are four rebonded second-layer atoms. Three vacancy lines, running vertically in the picture, are labeled as VL1 to VL3. Also defined are the h axis; the distance between two neighboring vacancy lines, n; the separation l of two vacancies on adjacent dimer rows. (From ref 48.)

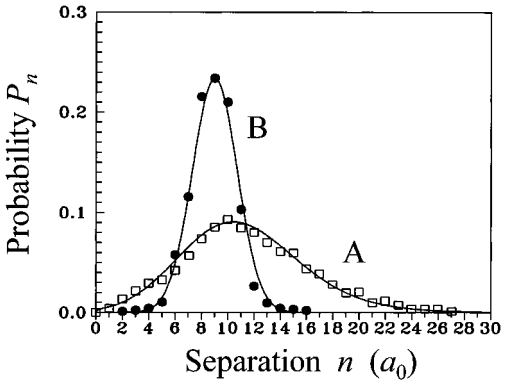

Figure 4. Separation probability distributions P_n of adjacent dimer vacancies on the same dimer row at (A) $\theta_{Ge} \approx 0.8$ ML and (B) $\theta_{Ge} \approx 1.6$ ML, respectively. (From ref 49.)

stress in the overlayer is not relieved enough; if they are too close, the stress is "over-relieved". Effectively, this balancing of tensile and compressive stresses amounts to a short-range repulsive, long-range attractive interaction between DVs on the same dimer row, as shown directly by total-energy calculations.[22,40]

The thermal fluctuation of DVs causes n to have a distribution function $P_n(n)$, peaked at an optimal value of n. [$P_n(n)$ is the probability of finding dimer vacancies on the same dimer row separated by n dimers]. Figure 4 shows two such distribution functions, for $\theta_{Ge} = 0.8$ and 1.6 ML, respectively.[49] They are determined by counting n in individual dimer rows of many STM images like those shown in Figure 2. As the Ge coverage increases, more vacancies are created to relieve the increasing misfit strain. Consequently, the optimal value of n in Figure 4 decreases with increasing Ge coverage, from ~11 at 0.8 ML to ~9 at 1.6 ML, consistent with an earlier LEED measurement[44] and a recent theory.[22] (During Si/Ge alloy growth, the changing n reflects the different amount of Ge surface segregation.[47]) In addition, as the VLs are getting closer to each other (at smaller n's), the thermal fluctuations in a given VL are suppressed by the stronger confinement produced by neighboring VLs, so the width of the distribution function decreases with increasing coverage. For $\theta_{Ge} = 0.8$ ML, the P_n distribution (curve A) is broad and asymmetric and can be fitted by a model of noninteracting, freely meandering line defects,[51] suggesting a very weak DV−DV interaction; for $\theta_{Ge} = 1.6$ ML, the distribution (curve B) is narrow and symmetric and can be nicely fitted by a Gaussian function (see discussion below). Energetics calculations[22] of the $(2\times n)$ structure show trends in the optimal value of n and its confinement potential as a function of Ge coverage similar to those in typical experiments,[48−50] which are at quasi-equilibrium conditions at which Si/Ge interlayer mixing is minimal (see section VI for details). The theory[22] further shows that, at true equilibrium, there should be considerable intermixing of Ge into the top few Si layers, affecting both the value of n and the shape of its confinement potential. A recent experiment[52] demonstrates that it is possible to obtain different n values and distribution functions $P_n(n)$ for the same Ge coverage by using different growth and annealing procedures to induce Si/Ge

intermixing.

When DVs are on different dimer rows, the interaction between them must be short-range attractive, on the basis of the very fact that they prefer to order into nearly straight VLs.[48] The dependence of the interaction potential energy on the separation of DVs on neighboring dimer rows has been calculated from first principles;[30] the results are in good agreement with experiment.[48] Along each VL thermal excitation displaces the DVs from the mean position, giving rise to a second probability distribution, $P_h(h_i)$, where h_i specifies the position of a vacancy on the i-th dimer row in a VL, measured from the mean position of this VL (see Figure 3). Because STM images are typically limited to about 400 Å × 400 Å in order to maintain atomic resolution in viewing the dimer vacancy,[48] it is impossible to locate accurately the mean position of a VL solely from these images and therefore, unlike the P_n distribution, the P_h distribution cannot be obtained directly from the images. However, analysis[48,50] shows that the meandering of neighboring VLs is uncorrelated; the probability of exciting a vacancy−vacancy displacement in a given VL is independent of the existence or the direction of the displacements in the neighboring VLs (see Figure 3). Consequently, the distribution P_n is simply a convolution of two independent probability distributions: $P_h(h_{1,i})$ and $P_h(h_{2,i})$, where $h_{1,i}$ and $h_{2,i}$ are respectively the h coordinates of two neighboring DVs on dimer row i. Once the P_n distribution is measured from the images, P_h can be obtained by deconvolution. The analysis[48,50] further shows that, within the same VL, the displacements of DVs on different dimer rows show no correlations. The profile of a VL can be equivalently viewed as the trace of an 1D random walk within an external potential $V(h)$. If the potential is assumed to be quadratic, $\beta V(h) = (1/2)kh^2$, where $\beta^{-1} = (k_B T)$, k_B is the Boltzmann constant, T is the equilibrium temperature, and k is an effective force constant, the trace follows precisely a Gaussian distribution.[53,54] In Figure 4, the P_n distribution for $\theta_{Ge} = 1.6$ ML (curve B), has been fitted by a Gaussian function with a width of $w_n = 1.67a_0$.[48] The deconvolution yields then a Gaussian form for P_h as well with a width of $w_h = w_n/\sqrt{2} = 1.20a_0$.

2. Interactions between Dimer Vacancies

The noncorrelated meandering of neighboring VLs justifies a mean-field approximation, which simplifies the 2D interaction problem of DVs to a 1D model.[48,50] The system consists of a collection of VLs, each moving in an effective potential, $V(h)$, representing the collective effect of all the other VLs. The problem reduces then to understanding the behavior of a single VL in an external field $V(h)$. Moreover, the relative displacement of DVs in a VL is independent of the existence or the direction of any other relative displacement in the same VL. Therefore, only nearest-neighbor interactions along a line of DVs need to be considered.[48,50] Under these constraints, the problem can be solved exactly within the framework of transfer matrix theory.[48,50]

The Hamiltonian of the VL is

$$H[\{h_i\}] = \sum_i E(h_i,h_{i+1}) + \sum_i V(h_i) \qquad (2)$$

where each pair of adjacent DVs has an interaction energy $E(h_i,h_{i+1})$ that depends only on their separation l: $E(h_i,h_{i+1}) = E(l)$. We introduce the transfer matrix, **T**, whose elements are given by

$$T_{h_1,h_2} = \exp\{-\beta E(h_1,h_2) - {}^1/_2\beta[V(h_1) + V(h_2)]\} \quad (3)$$

Using eqs 2 and 3, we can express the probability of finding a relative displacement l as

$$P(l) = \frac{2}{Z}\sum_{\{h_i\}}\delta(h_1 - h_2 - l)T_{h_1h_2}T_{h_2h_3}\cdots T_{h_{N-1}h_N}T_{h_Nh_1} \qquad (4)$$

where Z is the partition function. After some algebra, eq 4 leads to

$$P(l) = \lambda_m{}^{-1}\exp[-\beta E(l)]\sum_{h_1}\exp\{-{}^1/_2\beta[V(h_1) + V(h_1 - l)]\}\sqrt{P_h(h_1)P_h(h_1 - l)} \quad (5)$$

where λ_m is the largest eigenvalue of the transfer matrix. Inserting the quadratic form of $V(h)$ and the Gaussian form of P_h into eq 5, we obtain

$$\beta E(l) = -\ln\frac{P(l)}{2P(0)} - {}^1/_8(k + w_h{}^{-2})l^2 \qquad (6)$$

Equation 6 provides the first key relationship from which the dependence of the interaction energy $E(l)$ between two DVs on neighboring dimer rows on their separation l can be extracted. Without the second term on the right hand side, it is the expression for a Boltzmann distribution with no external confinement potential $V(h)$. The effect of the confinement, represented by the second term, vanishes when $k = 0$ and $w_h \to \infty$, for a free random walk. In this equation, values of w_h and $P(l)$ are obtained from the STM images, but the strength of the mean-field potential, k, is yet to be determined. In order to extract the values of both $E(l)$ and k simultaneously we must invoke a second relationship.[48,50] This second relationship is provided by self-consistency in the Metropolis Monte Carlo simulations to generate the equilibrium configurations of the VLs using the Hamiltonian defined by eq 2, with the second term on the right-hand side given by $\beta V(h) = ({}^1/_2)kh^2$. For each trial value of k, $E(l)$ is calculated according to eq 6. The program generates equilibrium vacancy line configurations, from which the distribution $P_h(h)$ is calculated and compared to the experimentally determined $P_h(h)$ until a correct value of k is found so that the computer generated $P_h(h)$ converges to the experimental Gaussian distribution. Convergence is mandatory if the mean-field model is valid.[48,50]

The simulations[48,50] following this scheme yield $k = (0.075 \pm 0.008)a_0{}^{-2}$ for $\theta_{Ge} = 1.6$ ML. The corresponding interaction energy $E(l)$ between two DVs on adjacent dimer rows separated by l is plotted vs l in Figure 5. The interaction is attractive and short-

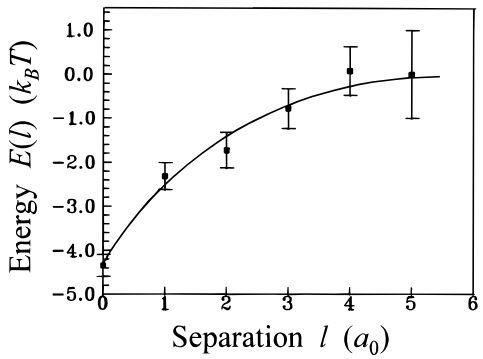

Figure 5. The interaction energy of dimer vacancies $E(l)$ on adjacent dimer rows vs their separation l. The solid curve guides the eye. (From ref 50.)

ranged; it becomes zero when the relative displacement between the DVs on neighboring dimer rows is beyond $4a_0$. The origin of the energy axis in Figure 5 is chosen so that $E(5) = 0$, indicating that we are using the energy of two well-separated, hence noninteracting, dimer vacancies as the energy reference. Assuming a temperature of 600 K at which the VLs in Figure 2 are at equilibrium, the strength of the attraction interaction, or equivalently the binding energy of two dimer vacancies, is about 215 meV.[48] These results are obtained for $\theta_{Ge} = 1.6$ ML. The interactions between DVs may depend on θ_{Ge} and the Si/Ge surface composition. Nevertheless, a recent first-principles calculation[30] of a surface with $\theta_{Ge} =$ 3 ML shows a strength and form of the short-range DV−DV attraction in neighboring dimer rows similar to that has been measured for $\theta_{Ge} = 1.6$ ML.

The physical origin of this attraction is a delicate relaxation of the local atomic structure around the two neighboring dimer vacancies.[30,48] When a vacancy is created on the surface, atoms around it deform to find the lowest-energy configuration. For two close-lying vacancies, the local relaxation associated with each vacancy overlaps and interferes. By optimizing the atomic structure at different vacancy−vacancy separations, the strain energy, associated with the relative displacement of two neighboring DVs, is shown[30] to increase with increasing separation, leading to an effective attractive DV−DV interaction.

In the dimer row direction, the VL−VL interaction is short-range repulsive and long-range attractive. For the mean-field potential $V(h)$, which represents the collective effect of VL−VL interaction between a given VL and all the other VLs, it has a minimum at the mean position of a given VL. The leading term in the expansion of $V(h)$ at the minimum is therefore always quadratic, independent of the actual form of the VL−VL interaction. In the last section, the mean-field quadratic potential is determined from a self-consistent analysis of vacancy distribution functions, but the exact form of the VL−VL interaction is still unknown. Alternatively, this interaction can be obtained from total-energy calculations.[22,40] Figure 6 shows the calculated surface energy as a function of VL−VL separation [i.e., the n value in $(2\times n)$ reconstruction], at different Ge coverages for surfaces with and without Si/Ge interlayer mixing. For now, we will concentrate only on results without

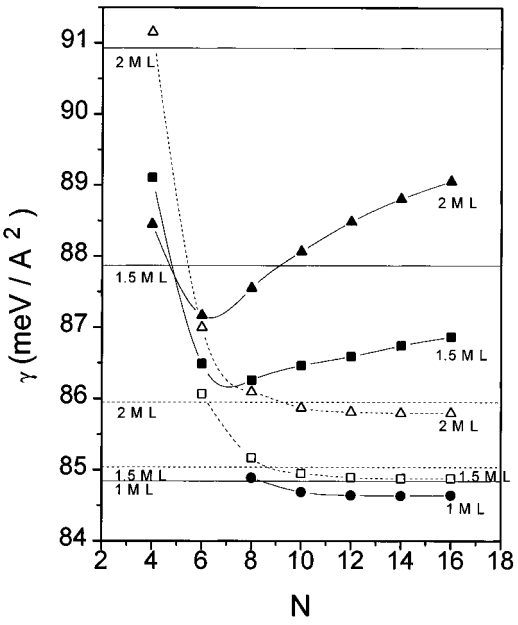

Figure 6. Surface energies for the $(2\times n)$ reconstruction at various coverages. Symbols are calculated values for 1 ML (solid circles), 1.5 ML (solid and open squares), and 2 ML (solid and open triangles) coverages, respectively. Solid (no interlayer mixing) and dashed curves (with interlayer mixing) are spline fits to the data. Horizontal lines mark the (2×1) surface energies for each individual surface. (From ref 22.)

Si/Ge mixing, which corresponds to the quasi-equilibrium obtained in typical experiments[23,48−50] (solid curves in Figure 6; the issue of intermixing will be discussed later). The minimum of the calculated potential (the optimal VL−VL separation, n) decreases with increasing Ge coverage. The potential well becomes deeper and narrower at larger coverages, suggesting that the statistical distribution of n will become narrower with increasing coverage. These results are in very good agreement with the observed distributions, $P_n(n)$, of separations of dimer vacancies on the same dimer row shown in Figure 4.

V. The Effect of (2×n) Reconstruction on Evolving Surface Morphology and Surface Stress Field

A. Reversal of Step Roughness

1. Experimental Observations

Scanning tunneling microscopy has revealed several interesting changes in surface morphology with the deposition of Ge[23,49,50] that accompany the development of the $(2\times n)$ reconstruction. A very distinct one is the reversal of relative roughness of the two types of steps on the surface.[49] When Si(001) is miscut at small angles with the normal tilted toward the [110] direction, two types of single-atomic-height steps form. The smooth S_A step is parallel to the upper-terrace dimer rows, while the rough S_B step is perpendicular to them.[55−57] Ge adsorption drastically changes the morphologies of both types of steps, leading to a reversal of their relative roughness.[49,50]

In the discussion below, we follow that of refs 49 and 50. Figure 7 demonstrates the progressive reversal of the step roughness induced by Ge adsorp-

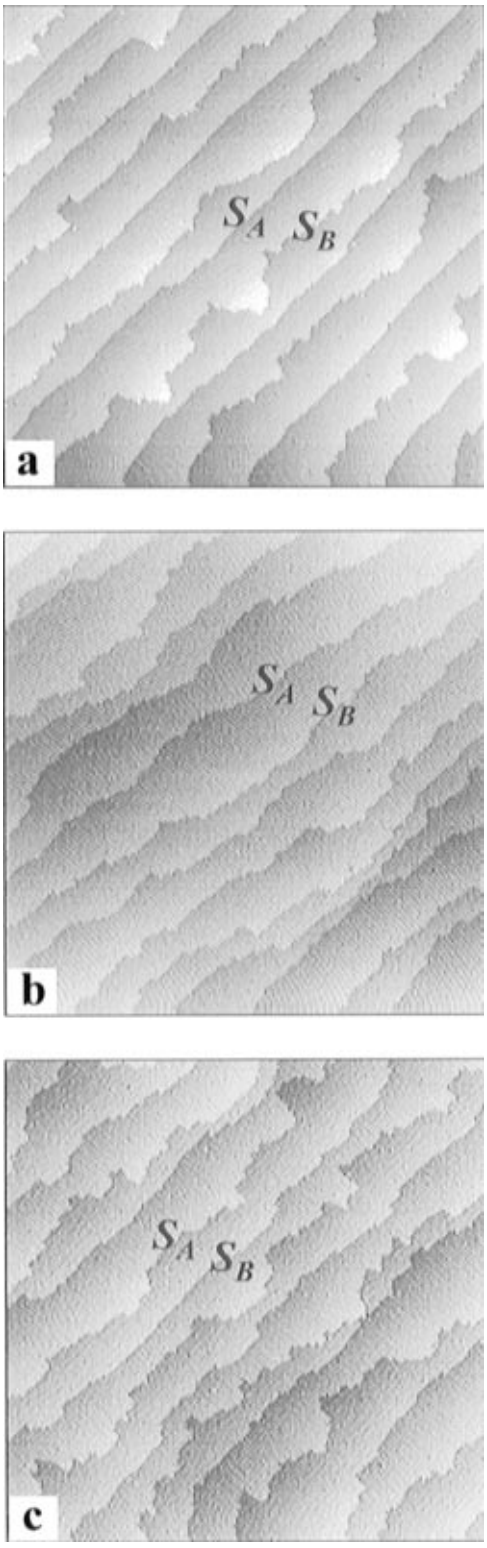

Figure 7. STM images (3000 Å × 3000 Å) of vicinal Si(001) surface 0.3° miscut toward [110]. (a) Clean surface; (b) Ge-covered, with $\theta_{Ge} \approx 0.8$ ML; (c) Ge-covered, with $\theta_{Ge} \approx 1.6$ ML. The two types of single atomic height steps (nominal) S_A and S_B are denoted. The staircase is down from upper left to lower right. (From ref 49.)

tion on vicinal Si(001).[49] Figure 7a is an STM image of the clean vicinal Si(001) surface miscut 0.3° toward [110]; the smooth S_A and rough S_B steps are clearly distinguishable. As the Ge coverage increases, the equilibrium step morphologies change in opposite directions: S_B steps become smoother and S_A steps rougher. At $\theta_{Ge} \approx 0.8$ ML, the two types of steps are visually equally rough (Figure 7b). Beyond this coverage the relative step roughness is reversed. At $\theta_{Ge} \approx 1.6$ ML, the S_B steps have become essentially straight except for a few long kinks, while the S_A steps are very rough (Figure 7c). An STM image at higher resolution for $\theta_{Ge} \approx 1.6$ ML is shown in Figure 8. Here the dimer rows are clearly visible, confirming the identification of the S_A and S_B steps. The roughnesses of the steps exhibited in Figure 7a and 7c are also qualitatively different, that in Figure 7c being much more "jagged" or "boxy".

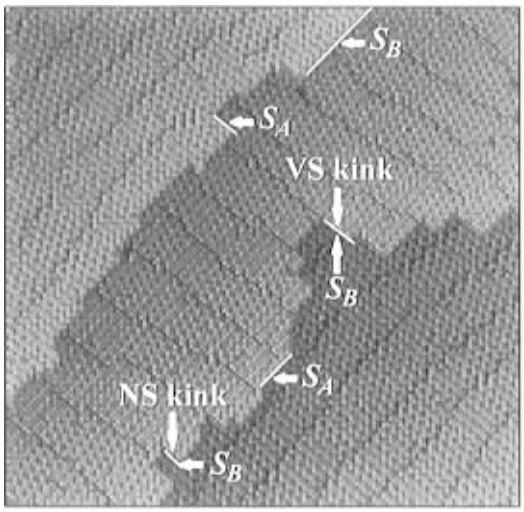

Figure 8. STM image (450 Å × 450 Å) of Si(001) covered with ~1.6 ML of Ge, showing atomically resolved structures of steps, kinks, dimer-vacancy lines, and dimer rows perpendicular to these lines. Vacancy-site (VS) and normal-site (NS) kinks are shown along the S_A step. (From ref 49.)

A step is roughened through the formation of kinks. A kink is defined by the sequential occurrence of two corners of opposite sense. Just as a step may have any height, a kink may have any length: the straight section between the corners defines the length of the kink. A quantitative analysis of kink excitations at steps is required in order to understand the relative roughness of steps. It has been shown[49,50] that there exists an intrinsic connection between the crossover process in relative step roughness and the ordering of the $(2\times n)$ reconstruction on terraces. The $(2\times n)$ reconstruction introduces a new type of kink along the S_A steps; it also confines the meandering of the S_B steps as a result of vacancy-step interaction. Ge−Si bonds additionally modify the kink energies. In the following, we provide a quantitative discussion of these effects, which act together to induce the reversal of the relative step roughness and to modify kink and step energies, as the Ge coverage increases.

2. Vacancy-Step Interaction and Its Effect on Kink and Step Energies

For clean Si(001), the relative roughness of S_A and S_B steps simply reflects their step energies.[56,57] A kink in the S_B step is just a segment of S_A step; for a rough S_B step the total length of S_B segments is conserved, but the length of S_A segments increases as the step gets rougher. Conversely, a rougher S_A step introduces more S_B segments. At thermal equilibrium the step free energy is minimized at a cost in step energy balanced by an increase in entropy.

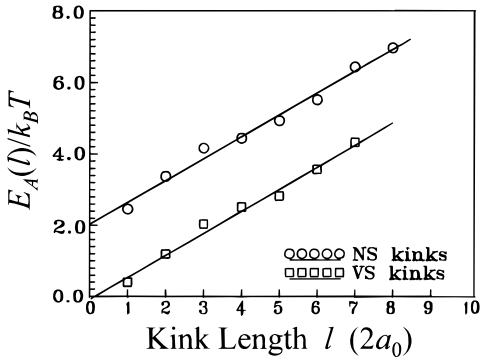

Figure 9. Dependence of the kink energies on kink length for both types of kinks along the nominal S_A step, for $\theta_{Ge} \approx 1.6$ ML. The data can be fitted by two straight lines, with the same slope ϵ_{SB} and different intercepts. (From ref 49.)

Because the formation energy per unit length of an S_A step is less than that of an S_B step,[55−57] the cost in making S_A segments is less, and therefore the S_B step is rougher. In addition, there is a cost in corner energy, which is the same on both steps.

For Ge-covered Si(001), the situation becomes more complex because of the presence of many VLs from the $(2\times n)$ reconstruction. A nontrivial modification of kink energy analysis is necessary to understand why the equilibrium step roughness for both types of steps is changed with increasing θ_{Ge}. The VLs introduce two new features along the steps. First, along the S_A steps, kinks can form with much higher probability at the sites at which the VLs terminate. Because of the difference in local bonding, these kinks must have energies different from those at the normal sites, where there are no DVs. We differentiate them as vacancy-site (VS) kinks and normal-site (NS) kinks (Figure 8). Second, since the VLs on the upper terrace are parallel to the S_B steps, they may limit the possible degree of the S_B step meandering. In that sense the step can be considered as simply another VL, whose meandering is confined by its neighboring VLs, as shown above. In addition, the existence of Ge atoms in the overlayer creates Si−Ge and Ge−Ge bonds, which may occur at the steps and thus alter the step energies.

A quantitative analysis[49,50] of kink excitations on Ge/Si(001) with $\theta_{Ge} \approx 1.6$ ML has been carried out to determine the kink and step energies on a surface with reversed step roughness and to compare them to those of clean Si(001). For the S_A steps, the VS and NS kinks need to be counted and analyzed separately. The kink excitations for Ge-covered Si(001) are independent [as for clean Si(100)], i.e., no neighboring kink−kink correlation exists.[49,50] Consequently, the number $N(l)$ of kinks of length l must follow a Boltzmann distribution: $N(l) \propto \exp[-\beta E(l)]$, where $E(l)$ is the excitation energy of kinks of length l. By plotting $-\ln[N(l)/2N(0)]$ vs kink length l, the kink energy is extracted as a function of kink length. The results are shown in Figure 9 for both VS and NS kinks. The data can be fitted with straight lines, i.e., $E_A(l) = l\,\epsilon_{SB} + C_A$. The two lines have the *same* slope, $\beta\epsilon_{SB} = 0.62 \pm 0.06/2a_0$), but *different* intercepts, $\beta C_A^{VS} = 0.0 \pm 0.3$ and $\beta C_A^{NS} = 2.0 \pm 0.3$. Using an equilibrium temperature of 600 ± 100 K, estimated for this surface, the common slope gives $\epsilon_{SB}(\theta_{Ge} \approx 1.6\text{ML}) = 32 \pm 5$ meV/$(2a_0)$, substantially smaller than that of clean Si(001).[56,57]

The same slope simply reflects a single value of ϵ_{SB} for the S_B step energy per unit length $2a_0$, as expected for both types of kinks, because each VS and NS kink contains a section of S_B step. The difference in intercepts, i.e., the corner energies, C_A^{VS} and C_A^{NS}, results from the difference in local bonding at the inner corner of the two types of kinks: for every VS kink a dimer is missing at the inner corner, but this is not the case for a NS kink (see Figure 8). The vanishing corner energy of VS kinks implies a near-complete relaxation at the inner corner of a VS kink, leading to the lower overall energy of the VS kink relative to the NL kink and hence a higher probability of kink excitation at the vacancy sites. Direct counting of both types of kinks[50] confirms this conclusion. Because of their low formation energy, kinks are expected with high probability at the termination sites of VLs on the S_A steps. As θ_{Ge} increases, the number of VLs increases, providing more VS kinks and thus greater opportunity for the S_A steps to develop roughness.

The scenario for the S_B steps is totally different from that for the S_A steps. We recall that the S_B steps become smoother as θ_{Ge} increases from 0 to about 1.6 ML, implying that kinks become *harder* to create along these steps. In section IV.B.2, we descibed how the existence of the intrinsic vacancy-vacancy interactions on the Ge-covered Si(001)-$(2\times n)$ surface leads to a strong confinement of the meandering of a given VL by the presence of all the other VLs. Because an S_B step, parallel to the VLs on its upper terrace, is essentially the same as a VL judged from the point of view of the local bonding geometry, it is natural to expect this step to be subjected to a confinement similar to that imposed on all the VLs on terraces, forcing it to smooth.[49,50] In order to extract the intrinsic kink excitation energy from the meandering of the S_B steps, the effect of this confinement must be removed.

As for the meandering of VL, analysis[49,50] confirms that the meandering of an S_B step, for $\theta_{Ge} \approx 1.6$ ML, produces a Gaussian distribution function $P_x(x)$ of its excursion x perpendicular to the step (with a width of $w_x \approx 2.6a_0$), which implies that the leading term of the effective confinement potential has a quadratic form, $\beta V(l) = (1/2)gl^2$, where g is an effective force constant (see section IV.B.2). Also, the correlation between the meandering of the S_B step and its neighboring VL is statistically negligible so that a mean-field approximation is applicable. Therefore, the solution of eq 6 for the energy of a DV displacement in a VL can be readily transformed to the kink excitation energy in the S_B step

$$\beta E_B(l) = -\ln\left[\frac{N_B(l)}{2N_B(0)}\right] - {}^1/_8(g + w_x^{-2})l^2 \qquad (7)$$

where the first term is just the usual Boltzmann distribution with $N_B(l)$ being the kink length distribution on the S_B step measured from STM images and the second term is the energy that describes the effect of the confinement.

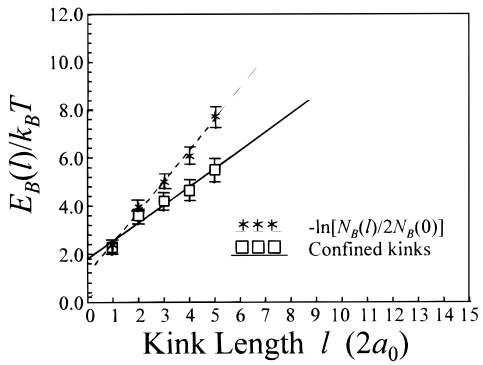

Figure 10. Dependence of the kink energy of the S_B step on kink length, for $\theta_{Ge} \approx 1.6$ ML. With the confinement, the kink energy (squares) is fitted by a solid line, whose slope is ϵ_{SA}. Without the confinement, the data are also plotted (asterisks), using a Boltzmann distribution with $N(l)$, the total number of confined kinks of length l, together with a linear fit (dashed line). (From ref 49.)

A plot ignoring the second term of eq 7[49] gives the stars in Figure 10. A linear fit (dashed line) to $E_B(l) = l\,\epsilon_{SA} + C_B$ gives $\beta\epsilon_{SA} = 1.3 \pm 0.1/(2a_0)$, a value almost two times that for clean Si(001),[56,57] which cannot be explained on physical grounds. The corner energy obtained in this way, $\beta C_B = 1.2 \pm 0.3$, is much smaller than βC_A^{NS}; the corners are identical, the values should be similar. These inconsistencies demonstrate the need to consider the confinement by VLs, i.e., the complete eq 7. Because the value of g is not *a priori* known, Metropolis Monte Carlo simulations are used to generate equilibrium kink configurations (see section IV.B.2), from which the distribution $P_x(x)$ is calculated and compared to the measured one until they converge.[49] This procedure yields $g \approx 0.04\ a_0^{-2}$. The corresponding values of $E_B(l)$ are plotted in Figure 9 as the squares. Now a linear fit (solid line) gives the true S_A step energy, $\beta\epsilon_{SA} = 0.7 \pm 0.1/(2a_0)$. The difference in the two lines in Figure 10 (the second term in eq 7) describes exactly the contribution of the confinement energy, which makes long-kink formation costly, leading to straightening of the S_B step.[49] The value of ϵ_{SA} here for $\theta_{Ge} \approx 1.6$ ML is only slightly smaller than that for clean Si(001),[56,57] in contrast to the large decrease observed for ϵ_{SB}, suggesting that the energy of an S_A step (the side of dimer rows) is less affected by Ge incorporation than is the energy of an S_B step (the end of dimer rows). The corner energy, $\beta C_B = 1.8 \pm 0.4$, now is within error bars the same as βC_A^{NS} obtained above, as it should be. Thus, after inclusion of the confinement effect, physically reasonable values of kink energetics of the S_B steps and in turn the S_A step formation energy are obtained.

In general, as first demonstrated by the analysis of step meandering on a high-miscut Si(001) surface,[58] when the terrace width becomes comparable with the longest kink length, the confinement effect on step meandering due to step−step interaction is no longer negligible, and it becomes inadequate to extract the kink energy from a simple Boltzmann relation. The confinement effect on step and vacancy-line meandering is expected to be a common phenomenon that should exist on other surfaces containing steps and/or vacancy lines; the confinement can arise from step−step, step−VL, and/or VL−VL elastic interactions. The method that has been developed to treat such confinement[48−50,58] will be generally applicable as well. For example, inclusion of the confinement will likely improve the determination of step energies in previous studies (e.g., GaAs(110),[59] GaAs(001),[60] and Ge-covered GaAs(001)[61]) that have treated step roughening without taking into account the confinement effect.[48]

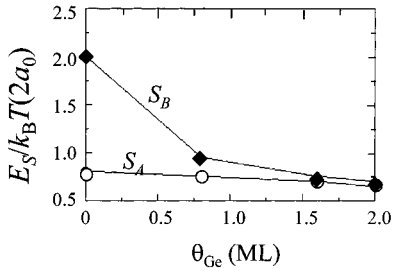

Figure 11. Dependence of the S_A (open circles) and the S_B (solid diamonds) step energies on the Ge coverage. (From ref 50.)

3. Dependence of Step Energies on Ge coverage

The above analysis for $\theta_{Ge} \approx 1.6$ ML can be extended to other coverages. Figure 11 illustrates the dependence of the step energies on the Ge coverage for both types of steps.[50] Both step energies decrease monotonically as θ_{Ge} increases: for the S_A step, it decreases slightly from the original value of $\epsilon_{SA} \approx 0.04$ eV/$(2a_0)$; for the S_B step, it decreases substantially from $\epsilon_{SB} \approx 0.10$ eV/$(2a_0)$ for clean Si(001) to $\epsilon_{SB} \approx 0.03$ eV/$(2a_0)$ for ≈ 1.6 ML Ge-covered Si(001). The large decrease in ϵ_{SB} but not in ϵ_{SA} is reasonable because the formation of S_B steps involves rebonding of second-layer atoms and large bond distortion, so it becomes more sensitive to Ge incorporation. In contrast, the corner energies of all the kinks do not change magnitudes with increasing θ_{Ge}, demonstrating the very localized nature of the corner effect.

On a strained surface, the step energy contains mainly two contributions. One is positive and local, resulting from bond distortion along the step. The other is negative and nonlocal, resulting from strain relaxation associated with the creation of the step. Both are likely to contribute to the monotonic decrease in the step energy as the Ge concentration is increased in the uppermost layers. First, because the strength of a Ge−Ge bond or a Ge−Si bond is weaker than that of a Si−Si bond, an overall smaller step energy is expected as Si−Si bonds are replaced by Ge−Ge and Ge−Si bonds. Second, at higher θ_{Ge}, the surface is more strongly strained, and the elastic energy released by the creation of a step is larger because it relaxes more strained bonds, producing an increasingly negative second term that reduces the magnitude of the step energy. The joint effect of both accounts for the observed decrease in ϵ_{SA} and ϵ_{SB}, although the magnitude of the effects may differ on different steps, as shown in Figure 11.[50]

Because STM cannot yet differentiate between Ge and Si atoms, it is, at the moment, not possible to extract detailed information on the local atomic structure and composition and hence to interpret the dependence of step energies on θ_{Ge} in more detail.

Step energies have been calculated only for clean Si(001), using semiempirical methods;[55,62] those are in reasonably good agreement with experiment.[56,57] A calculation of step energies for Ge-covered Si(001) is not yet available, because the presence of the $(2\times n)$ reconstruction and the uncertainty in Si/Ge surface composition make the calculation too complex.

Although both step energies decrease with increasing θ_{Ge} (especially the S_B steps), the change of step energies is not the main cause for the reversal of relative step roughness. Instead, the S_A steps are roughened by the VLs inducing a high probability of kink formation when they terminate on the S_A steps; the S_B steps are straightened by confinement of meandering via the VLs. However, the reduced step formation energy at high Ge coverage may induce other surface morphological instabilities. When step energies are sufficiently low, the strained Ge overlayer is thermodynamically unstable against the formation of extra steps, leading to a surface roughening process via 2D islanding,[7,8,23,50,63,64] i.e., formation of a stress-domain structure.[11,12,65] STM images[7,8,50,64] show that at a Ge coverage of about 2 or 3 ML, large $(2\times n)$ terraces break up into stripes of 2D islands, separated by trenches that are a several dimer rows wide. The islands maintain their $(2\times n)$ reconstruction; their width, on average, is only a few times that of the width of trenches between them, seemingly in accordance with the general size relation of stress domains established by theory.[65]

B. Reversal of Surface Stress Anisotropy

Adsorption of Ge modifies greatly the intrinsic surface stress field of Si(001) by lattice mismatch-induced strain and by strain-induced changes in surface structure and surface morphology [e.g., the $(2\times n)$ reconstruction]. For clean Si(001), the intrinsic surface stress is highly anisotropic (see section II). This stress anisotropy manifests itself on a vicinal surface as alternating (2×1) and (1×2) stress domains. The change of the relative populations of the two domains in response to an external stress can be measured to determine quantitatively the value of surface stress anisotropy.[13] Such measurements have also been carried out on Ge-covered Si(001)[21] surfaces that have been annealed to achieve the quasi-equilibrium morphologies described earlier, revealing a reversal of surface stress anisotropy with increasing Ge coverage.

Surfaces with different Ge coverages are imaged by STM under the influence of a given external compressive stress.[23] By comparing the responses (i.e., the changes of relative population of the (2×1) and (1×2) stress domains) to the same external stress for different θ_{Ge}s, one can not only observe qualitative changes of surface stress with increasing θ_{Ge} (in particular, the sign of the stress anisotropy), but also determine quantitative values of stress anisotropy with increasing θ_{Ge} by employing a theoretical model.[12,13]

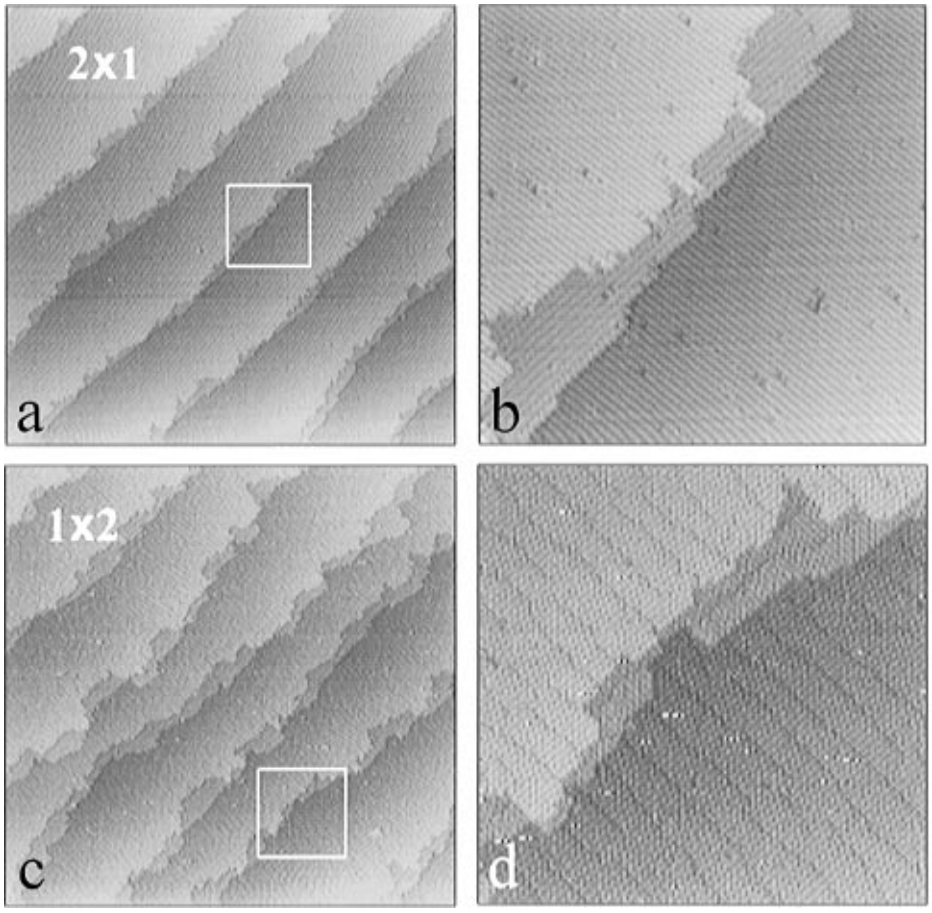

Figure 12. STM images (3000 Å × 3000 Å) of the equilibrium terrace structures of (a) clean and (c) Ge-covered ($\theta_{Ge} \approx 1.6$ ML) vicinal Si(001) 0.3° miscut toward [110] under applied compressive stress. Parts b and d are enlargements of the square area in a and c with dimer-row resolution. (From ref 23.)

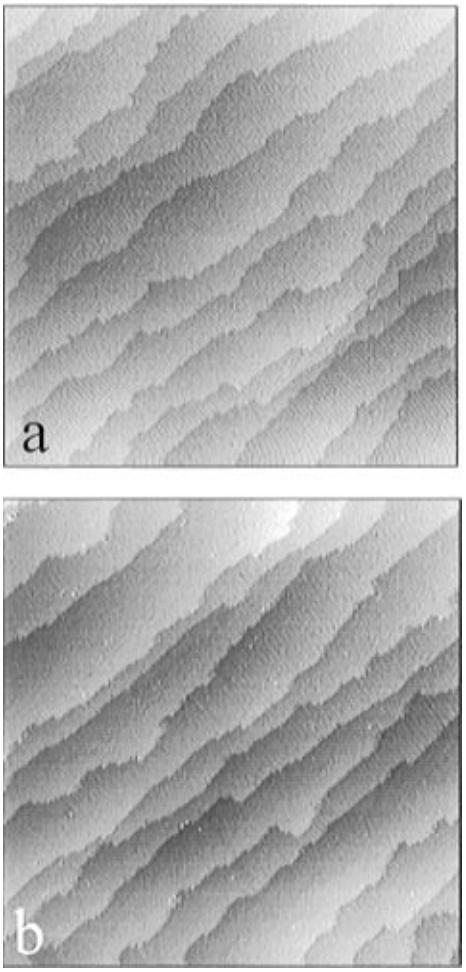

Figure 13. STM images (3000 Å × 3000 Å) of the equilibrium terrace structures of Ge-covered ($\theta_{Ge} \approx 0.8$ ML) vicinal Si(001) 0.3° miscut toward [110], (a) before and (b) after applying compressive stress to the sample. (From ref 23.)

Figure 12 shows the changes in the relative populations of (2×1) and (1×2) terraces induced by the external stress. For clean Si(001) (Figure 12a,b) the (2×1) domains (with dimer rows perpendicular to the down steps) grow at the expense of the (1×2) domains when a compressive uniaxial stress is applied along the dimer-bond direction in the (2×1) domains. The S_B steps almost reach the S_A steps. Figure 12b is a high-magnification image of the square area within Figure 12a, providing a clear identification of the dimer rows and thus the types of steps and terraces. After the deposition of ~1.6 ML of Ge and using the *same* external stress, the (1×2) domains grow at the expense of the (2×1) domains (Figure 12c,d), opposite to the behavior of clean Si(001). Now the S_A steps almost reach the S_B steps. At an intermediate coverage, ~0.8 ML, the steps do not respond to the external stress;[23] neither terrace domain is favored, as shown in Figure 13.

The above observations imply that the intrinsic surface stress anisotropy reverses its sign with increasing Ge coverage. Quantitatively, because the basic features of the dimerized surface structure do not change with the adsorption of Ge [except for the formation of dimer vacancies and changes in step and corner energies (see sections II and IV.B)], the equilibrium terrace population should be determined by the same type of stress potential as proposed for clean Si(001):[11,12]

$$E(p) = -\frac{F^2(1-\nu)}{2\pi\mu\langle L\rangle}\ln\left[\frac{\langle L\rangle}{\pi a_0}\cos\left(\frac{\pi p}{2}\right)\right] \qquad (8)$$

where $E(p)$ is the intrinsic elastic energy per unit area in the surface strain field with the relative population of two domains [i.e., (2×1) and (1×2)] as $(1 + p)/(1 - p)$, $0 \le p \le 1$, ν and μ are the Poisson ratio and bulk modulus, F is the stress anisotropy, L is the average terrace width, and a is a microscopic cutoff length as discussed in section II. When an external uniaxial stress is applied, another energy term, $\epsilon pF/2$, due to the external strain (ϵ) induced in the sample and the existence of surface stress anisotropy, must be added to eq 8. The domain degeneracy is lifted by the applied stress, and the terrace population becomes asymmetric. For clean Si(001), the domain for which the applied compressive stress is in the dimer-bond direction is favored. Once F reverses, for the *same* applied stress, the domain asymmetry should be opposite. If $F = 0$, the terrace population will be independent of the applied stress.

The elastic potential in eq 8 is derived for striped phases with straight parallel boundaries[12] while actual steps fluctuate by forming kinks. However, the spacing between kinks along the steps (kink separation) is generally much smaller than the terrace widths for both clean Si(001)[6,13,56] and Ge-covered Si(001),[23,50] and the interaction due to the long-range strain field cannot "follow" these small-scale fluctuations. It has been shown that[13] each step can be divided into many "long" segments (compared with the small-scale step fluctuation), meandering independently under the influence of the mean-field potential $E(p)$. The step separation distribution $g(L)$ for segment ξ follows then a Boltzmann distribution:[13,23,50]

$$g(L) \propto \exp[-2\beta\langle L\rangle\xi E(p)] = [\cos(\pi p/2)]^K \qquad (9)$$

where $K = \beta\xi F^2(1-\nu)/\pi\mu$. To determine the values of F for various θ_{Ge}, the equilibrium terrace width distributions $P(L)$ are obtained from many STM images by measuring the distance between adjacent steps in line scans.[23,50] Figure 14 shows two such distributions for clean Si(001) and Si(001) covered with ~1.6 ML Ge. Using the Boltzmann fits to the distributions (see Figure 14), the absolute value of F can be readily extracted with its sign already determined earlier. In principle, we are able to get the value of stress anisotropy, F, for any θ_{Ge} (except for $\theta_{Ge} \approx 0.8$ ML, where $F \approx 0$) low enough so that the quasi-equilibrium structure remains layers and not clusters. For the deposition of pure Ge on Si(001) that limit is ~2−3 ML. Figure 15 shows F as a function of θ_{Ge} up to 2 ML. As θ_{Ge} increases, the magnitude of F (originally positive) decreases first and becomes zero at $\theta_{Ge} \approx 0.8$ ML, and then reverses its sign and increases. For the unstrained surface for $\theta_{Ge} \approx 0.8$ ML, the distribution $P(L)$ cannot be fitted by g(L). Instead, it can be nicely fitted by a "universal" terrace width distribution for noninteracting, free-wandering steps within a 1D quantum

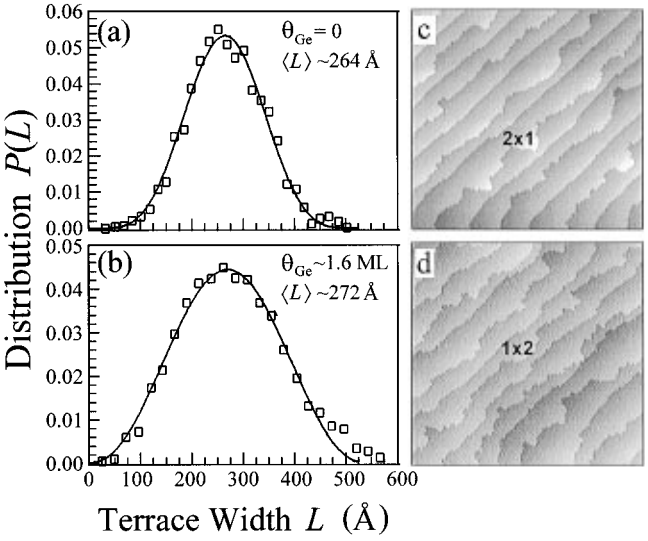

Figure 14. Equilibrium step separation distributions $P(L)$ for (a) clean Si(001) and (b) Si(001) covered with ~1.6 ML of Ge. The lateral resolution in each data point is limited by the pixel size in the image, here 20 Å × 20 Å. The solid curves are plots of a Boltzmann distribution $g(L)$ in the potential of eq 8 (see text). The best fitting yields $K \approx 4.7$ for clean Si(001) and $K \approx 2.2$ for $\theta_{Ge} \approx 1.6$ ML. (c and d) The corresponding STM images. (From ref 23.)

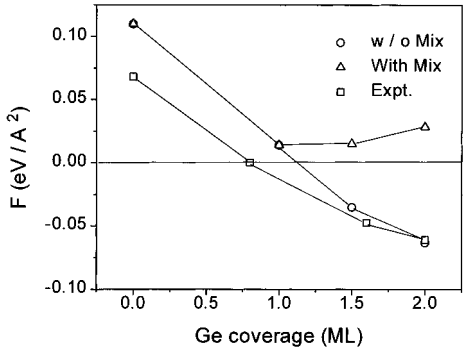

Figure 15. Surface stress anisotropy as a function of Ge coverage. Open triangles and circles are calculated results for the optimized $(2\times n)$ surface with and without interlayer mixing, respectively. Open squares are experimental data. Lines have been drawn to connect data points for clarity. (From ref 22.)

fermion model,[51] indicating that only entropic repulsion between steps exists at this θ_{Ge}. This conclusion is consistent with the vanishing stress anisotropy and hence vanishing stress potential found for $\theta_{Ge} \approx 0.8$ ML.

The physical origin of the reversal of surface stress anisotropy with increasing Ge coverage is believed to be caused mainly by the $(2\times n)$ reconstruction.[23] The larger lattice constant of Ge causes the surface stress to evolve, with increasing θ_{Ge}, gradually toward compression (or less tension) in both the dimer-row and dimer-bond directions. At the same time, the increasing concentration of rebonded dimer vacancies and their ordering tend to relieve the compressive lattice stress building up along the dimer rows, leading eventually to the reversal of stress anisotropy. This picture is confirmed by theoretical calculations[22] of surface energy and surface stress of $(2\times n)$ structures as a function of θ_{Ge}. The theory[22] further shows that the optimal surface structure (see Figure 6) and surface stress anisotropy (see Figure 15) depend strongly on the intermixing of Ge and Si in the surface and subsurface regions (which we will discuss in detail below). An experiment[66] has also been done to determine the difference in average stress between Ge-covered and clean Si(001) for different Ge coverages. By combining these with the measured stress anisotropies and the first-principles results for clean Si(001), one can determine the absolute values of each component of the surfaces stress tensor as a function of θ_{Ge}.[23,60]

VI. Ge/Si Intermixing

Despite extensive studies on surface morphology and surface stress of Ge-covered Si(001), there are still significant gaps in our understanding of the morphology and stress relationship in the Ge/Si(001) system. Fundamental in those gaps is the stoichiometry of the surface and subsurface regions as the coverage of Ge changes. The lack of knowledge of stoichiometry makes impossible a precise assignment of contributions to the morphology, energetics, and stress modification as Ge is added. STM has allowed us to characterize surface structures with atomic resolution and carry out quantitative measurements of surface energetics and surface stress, as demonstrated above, but it cannot yet distinguish between Si and Ge because of their similar atomic, electronic, and chemical properties. Nevertheless, semiquantitative information can still be inferred from STM measurements of surface structure (morphology) and surface stress by combining them with theories, as we discuss below.

A. Displacive Ge Adsorption

As Ge is deposited on Si(001), below 1 ML coverage, a surface layer consisting of a mixture of Ge and Si is believed to form through a displacive adsorption process.[67] Using deposition from a vapor source producing Ge atoms (typically called molecular beam epitaxy (MBE) but more properly evaporative deposition of atoms) at typical growth rates and temperatures of 500−700 °C onto a Si(001) substrate with typical small miscut, one would expect the layer to form via step-flow growth, i.e., the atoms have enough mobility to reach steps. Step flow is confirmed by the absence of islands on the terraces, as would be required in the island growth mode. The Ge adatoms are, however, not just incorporated at the steps but over the entire surface by exchanging places with Si atoms in the surface dimers to form Si−Ge mixed dimers or Ge dimers. The displaced Si atoms diffuse to and are incorporated at the steps to give the typical signature for step flow. This picture is inferred from experimental observations.[67,68] If the Ge adatoms were adsorbed at step edges, forming contiguous areas of Ge-covered Si that expand with increasing coverage, one would expect immediate formation of a $(2\times n)$ structure corresponding to 1 ML coverage in those areas, which would thus form a distinct phase coexisting with the bare Si areas. Instead, STM studies[6,44−50] show that dimer vacancies and then ordered vacancy lines gradually form uniformly on the entire surface upon Ge deposition. Other techniques[67] also observe gradual changes in surface structural and electronic

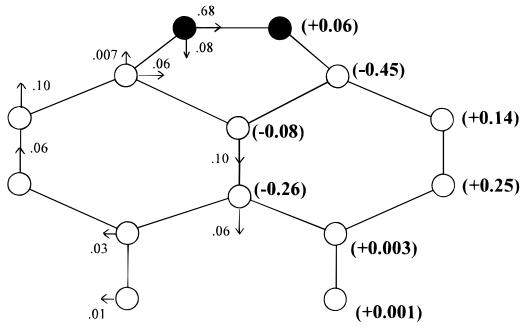

Figure 16. Schematic side view of (2×1) surface, projected to (110) plane. Solid circles are surface Ge atoms. Arrows mark the direction of atomic displacements. Numbers on the left hand side of the figure label the atomic displacements from their ideal bulk positions in Å. Numbers on the right hand side of the figure are atomic-level stresses. (From ref 22.)

characteristics, all over the terraces rather than observing two distinct areas of Ge-covered and bare Si surface.

The adsorption process of Ge on Si(001) is expected to have a strong impact on subsequent growth, but the atomistic mechanism for the proposed displacive exchange and the evolution of the surface compositional distribution are not known. Some recent developments (e.g., scanning tunneling spectroscopy[69] and Fourier transform infrared spectroscopy in combination with hydrogen titration[70]) that enable the differentiation between Ge and Si atoms will help us eventually to solve the problem. A recent STM experiment[31] shows that a single Ge dimer (or a Si−Ge mixed dimer) can be differentiated from a single Si dimer by their different dynamic motions at room temperature: a Ge dimer displays a rocking motion on top of a dimer row,[31] while a Si dimer displays a rotating motion.[32−35] The surface Si/Ge alloy composition can be determined by hydrogen titration,[70] using the relative intensities of Si−H and Ge−H vibrations measured by Fourier transform infrared−attenuated total reflection spectroscopy.

B. Ge/Si Interlayer Mixing in Subsurface Layers

Above 1 ML coverage, the surface is expected to be terminated completely by Ge, on the basis of surface energy considerations.[22,67] But the distribution of Ge in the subsurface regions is difficult to ascertain. A recent theoretical study[22] shows that the surface reconstruction and surface stress anisotropy of Ge-covered Si(001) depend strongly on the Ge distribution in the subsurface regions, in addition to the Ge coverage. Therefore, it is possible to establish, at least in a semiquantitative manner, the Ge subsurface stoichiometry above 1 ML coverage by matching the theory to the experimental results.[22]

The surface dimerization introduces not only an anisotropic surface stress but also a nonuniform stress field distribution in the subsurface region.[22,71] Figure 16 is a schematic view of the (2×1) structure at 1 ML Ge coverage, showing the calculated atomic displacements (left half) and effective atomic stresses (right half).[22,72] The surface dimer experiences a very small tensile stress. The second layer is under large compression. In the third and fourth layers, the sites beneath the surface dimers are under compressive stress and the sites between the surface dimers are under tensile stress. Below the fourth layer, there is virtually no stress. Because Si is smaller than Ge, lattice sites under compression favor Si occupancy and lattice sites under tension favor Ge. Stress provides a rather large thermodynamic driving force, beyond the usual entropic effects, for Si/Ge interlayer mixing. Given sufficient kinetics, the deposited Ge atoms would tend to migrate to tensile sites in the third and fourth layers to lower the overall surface energy. This mechanism has been proposed to be responsible for the growth of ordered Si−Ge alloy films on Si(001)[71] and for the oscillatory surface segregation in equilibrium bulk Si−Ge alloys.[73] Here, we discuss its effect on quasi-equilibrium surface structure and surface stress anisotropy.[22]

Surface energies for the (2×n) reconstructed Ge/Si(001) surface are calculated as a function of n for Ge coverages of 1, 1.5, and 2 ML, as shown in Figure 6. At 1 ML coverage, the Ge adatoms form the surface layer because the dangling-bond energy of Ge is much lower than that of Si. For coverages above 1 ML, two extreme cases are considered: one at the thermodynamic limit, the other at the kinetic limit. At the thermodynamic limit, for 1.5 ML coverage half a monolayer of Ge occupies the fourth-layer tensile sites with 1 ML on the surface; for 2 ML coverage half a monolayer each of Ge occupies both third- and fourth-layer tensile sites. As a limit of zero intermixing kinetics, all the deposited Ge adatoms are simply placed in the outer layers.

The optimal (2×n) reconstructions (the lowest energy points in Figure 6) at the three coverages considered here are all more stable than the corresponding (2×1) structures (horizontal lines in Figure 6), indicating a negative dimer vacancy formation energy (i.e., dimer vacancies are stable rather than metastable, see section IV.A). The deposited films allowing interlayer mixing (the thermodynamic limit, dashed lines in Figure 6) have lower surface energy and larger n values than the corresponding ones without interlayer mixing (solid lines). Obviously Ge segregation lowers the surface energy by occupying the favorable atomic sites to release surface stress. The relaxation of the stress in turn reduces the concentration of dimer vacancies, leading to surface structures with unchanged values of n at different coverages, in disagreement with the experiments,[44,49] which show a decreasing n with increasing Ge coverage. The calculations show that without interlayer mixing, the periodicity n gradually decreases with increasing Ge coverage, indicating that more and more vacancies are formed to relieve the misfit-induced compressive stress along dimer rows. Moreover, the potential well around the optimal periodicity becomes deeper and narrower at larger coverages, suggesting that the statistical distribution of n will become narrower with increasing coverage. Both these results are in agreement with experiments[44,49] (see section V.B.1 and Figure 4). The comparison between theory and experiment suggests that the thermodynamic limit is an incorrect assumption. This conclusion is confirmed by the calculations of stress anisotropy, as shown in Figure 15. In the thermodynamic limit, in addition to the formation of dimer

vacancies, the surface stress field is relaxed by interlayer mixing. As a result, the concentration of vacancies does not increase with increasing Ge coverage. The calculated surface stress anisotropy never changes sign, in disagreement with experiment. Without interlayer mixing, the theory shows that as Ge coverage increases, the surface stress anisotropy decreases and reverses in sign at about 1.1 ML, in good agreement with experiment.[23] We therefore conclude that films grown at typical experimental temperatures (500−700 °C)[23,48−50] are apparently unable to reach the *true* thermodynamic ground state, even when they are annealed for typical times of ∼1 h after growth in an attempt to achieve equilibrium, likely because the Si−Ge interlayer mixing is suppressed by a large kinetic barrier. It is believed that 2D equilibrium exists in the surface layer, but that equilibrium with the bulk is not established. The surface morphologies and surface stress tensors observed on these quasi-equilibrium films[23,48−50] are controlled by slow interdiffusion kinetics, at least for Ge coverages above 1 ML.

The above analysis demonstrates the possibility of deriving the Ge subsurface stoichiometry by matching the theory to the experimental surface structures and surface stress anisotropies. More detailed analyses[22] show that the actual amount of Ge mixing to lower layers is below 25.0% in the quasi-equilibrium films grown by those experiments.[23,48−50] The amount of interlayer mixing is expected to increase when the as-grown films are annealed at higher temperatures. Such intermixing can be monitored by observing the corresponding changes in surface structures and surface stresses. A recent STM study[52] shows that at ∼1.5 ML Ge coverage, high-temperature (∼760 °C) annealing changes the value of n in the surface reconstruction from 9 to 14. Because Ge evaporation at this temperature is negligible in the anneal time (∼ 2 min),[52] the decrease of dimer-vacancy concentration is speculated to be induced by additional Si/Ge interlayer mixing, as predicted by theory.[22] Several other measurements[74−76] have also suggested the segregation of Ge into the subsurface regions, up to the third and fourth layers, by growing and/or annealing at different temperatures.

VII. Transition from 2D to 3D Growth: Appearance of Coherent Facetted Islands

The equilibrium growth mode of Ge on Si is of the Stranski−Krastanov (SK) type. Ge initially grows layer by layer, forming a several-monolayer wetting layer, culminating eventually in the formation of dislocated islands that have the relaxed Ge lattice constant, with dislocations formed at the Ge−Si interface. Recent studies have discovered several interesting and unexpected growth processes before the formation of dislocated islands. The transition from 2D to 3D growth proceeds via complex kinetic pathways, characterized by the formation of coherent 3D faceted nano-crystallites.[63,64]

Because Ge has a lower surface energy than Si, Ge initially wets the Si substrate. For pure Ge deposited on Si(001), the strain relaxation mechanisms discussed above extend the thickness of the wetting layers up to 3 ML.[7,8,63,64,77−82] The misfit strain is partially relaxed by the $(2\times n)$ reconstruction, creation and morphological modulation of steps, and breakup of large terraces into 2D islands. The 3D nano-crystallites (referred to as "islands") start to form when $\theta_{Ge} \geq 3$ ML. They are coherent with the substrate lattice (i.e., free of dislocations between the substrate and the island)[63,80,81] and have well-defined facets.[63,64,81,83] In particular, STM has identified[63] these coherent 3D islands as hutlike with predominantly a prism shape (with canted ends), in some cases a four-sided pyramid, with perfect {105} facet planes on all four faces (see Figure 17). Their principal axes are strictly aligned along two orthogonal ⟨100⟩ directions.

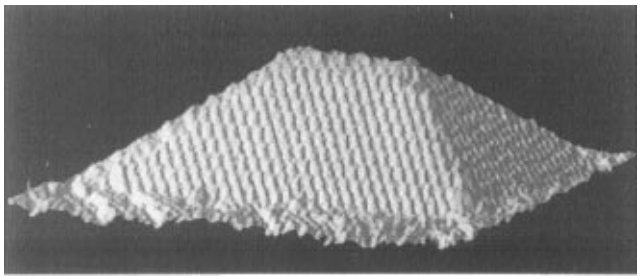

Figure 17. STM image of a single "hut" cluster in perspective view. The base dimensions are 400 Å × 200 Å. The height of the hut is 28 Å. (From ref 63.)

The four facets in these so-called "hut" islands[63] appear always with perfectly completed layers. This and the observation that the number density of the huts increases rapidly while their size grows slowly as the Ge coverage is increased indicate that the formation of huts is driven by the low surface free energy of {105} facet planes. Because hut clusters form preferentially at lower growth temperatures (< 500 °C) and because they transform completely to macroscopic islands after annealing at higher temperatures,[63] they are believed to be a metastable intermediate phase leading eventually to the formation of much larger stable noncoherent macroscopic islands[63,64,80,81] with less well-defined shape and structure. The kinetics of hut island formation are still unclear. The concentration at low growth temperatures of coherent hut islands is much higher than that of noncoherent macroscopic islands, indicating that huts are much easier to nucleate, with a lower formation barrier. Thus, hut clusters define the onset of the transition from 2D to 3D growth and provide a easier kinetic path for the ultimate formation of the equilibrium rough surface consisting of noncoherent macroscopic islands. The small formation barrier for huts can result from the low surface energy of their {105} facets (see discussion below). It is also suggested that ⟨100⟩ steps (running at 45° to the dimer-row direction), formed in the initial Ge layers, may lower the hut formation barrier by acting as nucleation sites.[63,84]

Theories show that under appropriate conditions, coherent islands can be not only energetically more stable than both the strained epitaxial films and dislocated islands,[85−87] but also kinetically favored over the nucleation of dislocations.[87] The coherent islands allow the partial relaxation of strain by elastic deformation at the expense of introducing extra surface area. In general, the strain relaxation

energy is proportional to the volume of the island (V), while the increase of surface free energy scales with the surface area ($V^{2/3}$). Considering an island of trapezoidal shape with a small facet angle, the total free energy of the island can be expressed as[87] $E = a\Gamma V^{2/3} - b\epsilon^2 V$, where a and b are coefficients related to the island facet angle, V is the volume of the island, ϵ is the misfit, and Γ is surface free energy anisotropy between the normal orientation and the beveled edge. Clearly, for a sufficiently large island (or an equivalent pit), formation of the island (or pit) is energetically favored. Kinetically, the thermal activation barrier is proportional to Γ^3/ϵ^{-4} for nucleating islands,[87] but scales as ϵ^{-1} for nucleating dislocations.[88] Thus, for large misfit (large ϵ), islands are kinetically favored over dislocations, while for small misfit, dislocations are favored.[87] The formation barrier depends also sensitively on surface free energy anisotropy (Γ). The smaller the value of Γ, the lower the barrier. It is likely that the difference in surface energy between the strained Ge(100) face and (105) face is rather small, making the nano-huts kinetically favorable over the macro-islands which contain other faces with surface energies much higher than that of the strained Ge(100) face. On the other hand, the macro-islands are energetically more stable than micro-huts by incorporating those faces with steeper facet angles to allow more strain relaxation,[83,87] which is consistent with the observation that micro-huts form preferentially at lower temperature and transform to macro-islands after annealing at higher temperature.[63] Also at higher temperature, Γ becomes generally smaller because of entropy; the islands will have multiple facets with less-defined overall shape and structure.[63] In order to grow thicker smooth films, it is possible to suppress the hut island formation by decreasing ϵ (e.g., lowering the concentration of Ge in a Si/Ge alloy that is deposited), decreasing Γ by, e.g., using surfactants[4] (which may also change surface diffusion), and/or growing at low temperature.

Recently, there has been a renewed intense interest[5,89−92] in the {105}-faceted hut islands[63] because of their potential applications as quantum dots. Similar huts form also during the growth of Si−Ge alloy films on Si(001) by both MBE and CVD. The most remarkable finding is that these islands, if grown in a SiGe/Si multilayer structure, self-organize into a superlattice with progressively improved uniformity in island size and spacing,[5,89,90] showing promise for obtaining the structure and order needed for electronic applications of quantum dot arrays.

VIII. Summary

STM has become a powerful surface tool not only for imaging evolving surface structures and morphologies but through them for determining quantitative values of surface energetics and stress. In this review, using the growth of pure Ge on Si(001) as a model system, we have presented a comprehensive picture of the effect of misfit strain on thermodynamic properties that become the driving forces for morphologies and other properties that influence the early stages of heteroepitaxy. The strain relaxation proceeds in steps via different relaxation modes. The analysis process and methods discussed here should be generally applicable to similar problems in a much wider range of systems.

On Ge-covered Si(001), strain relaxation begins with the formation of ordered dimer vacancies. The form and magnitude of the dimer vacancy−vacancy interaction can be determined by measuring and analyzing the vacancy distribution functions. The formation of vacancy lines changes the step energies and morphologies, reversing the relative roughness of two types of monatomic steps on Si(001). The response of surface morphology, for surfaces covered with different amounts of Ge, to an external uniaxial stress reveals an intriguing interplay of surface stress, structure, and stoichiometry. As strain increases with increasing film thickness, other modes of stress relief become important. In particular, a transition from 2D layers to 3D clusters, the classic transition predicted by Stranski and von Krastanov, must occur. This transition turns out to be very complex, beginning with a breakup of the 2D layers into smaller sections of 2D layer and a subsequent formation of coherent metastable 3D crystallites and only much later ending with relaxed larger-sized clusters as expected from the Stranki−Krastanov theory. The discovery, by STM, of this special kind of {105}-faceted coherent Ge island on Si(001) has provided new insights to the conventional Stranski−Krastanov theory. These microscopic "hut" islands also show great promises for future technological applications as quantum dot devices.

Formation of defects (vacancies, steps, etc.) and formation of coherent 3D islands are two typical strain-induced surface roughening processes. However, strain relaxation can have much richer manifestations. The form and process of surface roughening, i.e., the mode of strain relaxation, depend strongly on growth conditions (deposition rate, temperature, substrate miscut and orientation, alloy concentration, etc.) and can be affected by externally applied stress.[23,93] For example, on a vicinal surface, the bunching of steps created by miscut is the dominant relaxation mechanism during the growth of SiGe alloy on Si(001).[94,95] It has been shown[95] that there exists a generic step bunching instability of a strained vicinal surface, arising from the long-range elastic step−step attraction induced by lattice mismatch.[95] Such step bunching also leads to self-organization of step bunch arrays that are potentially useful for growing quantum wires.[96] While surface roughening, in general, prevents the growth of smooth films, it can be useful for fabricating nanostructures.[90] A good control of roughening processes through the manipulation of growth kinetics and surface thermodynamics, leading to self-organization of superlattices of quantum dots and quantum wires, has become an attractive route to nanofabrication.

IX. References

(1) See, for example: Whall, T. E.; Parker, E. H. C. J: *Materials Sci.. Materials in Electronics* **1995**, *6*, 249.
(2) Van der Merwe, J. H. J: *Appl. Phys.* **1963**, *34*, 117; **1963**, *34*, 123.
(3) Matthews, J. W.; Blakeslee, A. E. *J. Cryst. Growth* **1975**, *29*, 273; **1976**, *32*, 265.

(4) Copel, M.; Reuter, M. C.; Kaxiras, E.; Tromp, R. M. *Phys. Rev. Lett.* **1989**, *63*, 632. LeGoues, F. K.; Copel, M.; Tromp, R. M. *Phys. Rev. Lett.* **1989**, *63*, 1826.
(5) See, for example: *Physics Today* **1996**, *49*, No. 5, 22.
(6) Mo, Y. W.; Lagally, M. G. *Surf. Sci.* **1991**, *248*, 313. Mo, Y. W.; Kleiner, J.; Webb, M. B.; Lagally, M. G. *Phys. Rev. Lett.* **1991**, *66*, 1998. Mo, Y. W.; Kleiner, J.; Webb, M. B.; Lagally, M. G. *Surf. Sci.* **1992**, *268*, 275.
(7) Mo, Y. M.; Lagally, M. G. *J. Cryst. Growth* **1991**, *111*, 876.
(8) Lagally, M. G. *Jpn. J. Appl. Phys.* **1993**, *32*, 1493.
(9) Schlier, R.; Farnsworth, J. *J. Chem. Phys.* **1959**, *30*, 917.
(10) Tromp, R. M.; Hamers, R. J.; Demuth, J. E. *Phys. Rev. Lett.* **1985**, *55*, 1303; *Phys. Rev. B* **1986**, *24*, 5343.
(11) Marchenko, V. I.; Parshin, A. Y. *Zh. Eksp. Teor. Fiz.* **1980**, *79*, 257; *Sov. Phys. JETP* **1980**, *52*, 129.
(12) Alerhand, O. L.; Vanderbilt, D.; Meade R. D.; Joannopoulos, J. D. *Phys. Rev. Lett.* **1988**, *61*, 1973.
(13) Men, F.-K.; Packard, W. F.; Webb, M. B. *Phys. Rev. Lett.* **1988**, *61*, 2469. Webb, M. B.; Men, F.-K.; Swartzentruber, B. S.; Kariotis, R.; Lagally, M. G. *Surf. Sci.* **1991**, *242*, 23.
(14) Payne, M. C.; Roberts, N.; Needs, R. J.; Needels, M.; Joannopoulos, J. D. *Surf. Sci.* **1989**, *211*, 1.
(15) Meade, R. D.; Vanderbilt, D. In *Proceedings of the Twentieth International Conference on the Physics of Semiconductors*; Anastassakis, E. M., Joannopoulos, J. D., Eds.; World Scientific: Singapore, 1990; p 123.
(16) Garcia, A.; Northrup, J. E. *Phys. Rev. B* **1993**, *48*, 17350.
(17) Dabrowski, J.; Pehlke, E.; Scheffler, M. *Phys. Rev. B* **1994**, *49*, 4790.
(18) Shoji, K.; Hyodo, M.; Ueba, H.; Tatsuyama, C. *Jpn. J. Appl. Phys.* **1983**, *22*, 1482.
(19) Iwawaki, F.; Kato, H.; Tomitori, M.; Nishikawa, O. *Surf. Sci.* **1992**, *266*, 285.
(20) Fontes, E.; Patel, J. R.; Comin, F. *Phys. Rev. Lett.* **1993**, *70*, 2790.
(21) Cho, J.-H.; Kang, M.-H. *Phys. Rev. B* **1994**, *49*, 13670.
(22) Liu, F.; Lagally, M. G. *Phys. Rev. Lett.* **1996**, *76*, 3156.
(23) Wu, F.; Lagally, M. G. *Phys. Rev. Lett.* **1995**, *75*, 2534.
(24) Liu, F.; Lagally, M. G. In *The Chemical Physics of Solid Surfaces*; King, D. A., Woodruff, D. P., Eds.; 1997; v8.
(25) Srivastava, D.; Garrison, B. J. *Phys. Rev. B* **1992**, *46*, 1472.
(26) Roland, C.; Gilmer, G. H. *Phys. Rev. B* **1993**, *47*, 16286.
(27) Milman, V.; Jesson, D. E.; Pennycook, S. J.; Payne, M. C.; Lee, M. H.; Stich, I. *Phys. Rev. B* **1994**, *50*, 2663.
(28) Brocks, G.; Kelly, P. J.; Car, R. *Phys. Rev. Lett.* **1991**, *66*, 1729.
(29) Mo, Y. W.; Swartzentruber; Kariotis, R.; Webb, M. B.; Lagally, M. G. *Phys. Rev. Lett.* **1989**, *63*, 2393.
(30) Yu, B. D.; Oshiyama, A. *Phys. Rev. B* **1995**, *52*, 8337.
(31) Qin, X. R.; Lagally, M. G. *Phys. Rev. Lett.*, submitted for publication.
(32) Brocks, G.; Kelly, P. J.; Car, R. *Surf. Sci.* **1992**, *269/270*, 960. Brocks, G.; Kelly, P. J. *Phys. Rev. Lett.* **1996**, *76*, 2362.
(33) Toh, C. P.; Ong, C. K. *J. Phys. Condens. Matter* **1993**, *5*, 551.
(34) Zhang, Z. Y.; Wu, F.; Zandvliet, H. J. W.; Poelsema, B.; Metiu, H.; Lagally, M. G. *Phys. Rev. Lett.* **1995**, *74*, 3644.
(35) Bedrossian, O. J. *Phys. Rev. Lett.* **1995**, *74*, 3648.
(36) Theis, W.; Tromp, R. M. *Phys. Rev. Lett.* **1996**, *76*, 2770.
(37) Li, A. H. Personal communication.
(38) Tromp, R. M. Personal communication.
(39) Pandey, K. C. In *Proceedings of International Conference on the Physics of Semiconductors*; Chadi, D. J., Harrison, W. A., Eds.; Springer: Berlin, 1985.
(40) Tersoff, J. *Phys. Rev. B* **1992**, *45*, 8833.
(41) Roberts, N.; Needs, R. J. *Surf. Sci.* **1990**, *236*, 112.
(42) Wang, J.; Arias, T. A.; Joannopoulos, J. D. *Phys. Rev. B* **1993**, *47*, 10497.
(43) Hamers, R. J.; Köhler, U. *J. Vac. Sci. Technol.* **1989**, *A7*, 2854.
(44) Köhler, U.; Jusko, O.; Müller, B.; Horn-von Hoegen, M.; Pook, M. *Ultramicroscopy* **1992**, *42*−*44*, 832.
(45) Iwawaki, F.; Tomitiri, M.; Nishikawa. *Ultramicroscopy* **1992**, *42*−*44*, 895, 902.
(46) Croke, E. T.; Hauenstein, R. J.; Fu, T. C.; McGill, T. C. J. *Vac. Sci. Technol.* **1991**, *B9*, 2301.
(47) Butz, R.; Kampers, R. *Appl. Phys. Lett.* **1992**, *61*,1307; *Thin Solid Films* **1992**, *222*, 104.
(48) Chen, X.; Wu, F.; Zhang, Z. Y.; Lagally, M. G. *Phys. Rev. Lett.* **1994**, *73*, 850.
(49) Wu, F.; Chen, X.; Zhang, Z. Y.; Lagally, M. G. *Phys. Rev. Lett.* **1995**, *74*, 574.
(50) Wu, F. Ph.D. Dissertation, University of Wisconsin−Madison, 1996.
(51) Joos, B.; Einstein, T. L.; Bartelt, N. C. *Phys. Rev. B* **1991**, *43*, 8153.
(52) Li, A. H.; Liu, F.; Lagally, M. G. To be published.
(53) Fisher, M. E.; Fisher, D. S. *Phys. Rev. B* **1982**, *25*, 3192.
(54) Bartelt, N. C.; Einstein, T. L.; Williams, E. D. *Surf. Sci. Lett.* **1990**, *240*, L791.
(55) Chadi, D. J. *Phys. Rev. Lett.* **1987**, *59*, 1691.
(56) Swartzentruber, B. S.; Mo, Y.-W.; Kariotis, R.; Lagally, M. G.; Webb, M. B. *Phys. Rev. Lett.* **1990**, *65*, 1913. Swartzentruber, B. S. Dissertation, University of Wisconsin−Madison 1992.
(57) Zandvliet, H. J. W.; Elswijk, H. B.; Van Loenen, E. J.; Dijkkamp, D. *Phys. Rev. B* **1992**, *45*, 5965.
(58) Swartzentruber, B. S.; Kitamura, N.; Lagally, M. G.; Webb, M. B. *Phys. Rev. B* **1993**, *47*, 13432.
(59) Yang, Y.-N.; Trafas, B. M.; Siefert, R. L.; Weaver, J. H. *Phys. Rev. B* **1991**, *44*, 3218.
(60) Poon, K.; Maboudian, R.; Bressler-Hill, V.; Leonard, D.; Wang, X.-S.; Self, K.; Weinberg, W. H.; Petroff, P. M. *J. Vac. Sci. Technol.* **1993**, *B11*, 1374.
(61) Wang, X.-S.; Self, K.; Leonard, D.; Bressler-Hill, V.; Maboudian, R.; Petroff, P. M.; Weinberg, W. H. *J. Vac. Sci. Technol.* **1993**, *B11*, 1477.
(62) Poon, T. W.; Yip, S.; Ho, P. S.; Abraham, F. F. *Phys. Rev. Lett.* **1990**, *65*, 2161.
(63) Mo, Y. W.; Savage, D. E.; Swartzentruber, B. S.; Lagally, M. G. *Phys. Rev. Lett.* **1990**, *65*, 1020. Mo, Y. W. Ph.D. Dissertation, University of Wisconsin−Madison, 1991.
(64) Tomitori, M.; Watanabe, K.; Kobayashi, M.; Nishikawa, O. *Appl. Surf. Sci.* **1994**, *76/77*, 322.
(65) Zeppenfeld, P.; Krzyzowski, M.; Romainczyk, C.; Comsa, G.; Lagally, M. G. *Phys. Rev. Lett.* **1994**, *72*, 2737.
(66) Schell-Sorokin, A. J.; Tromp, R. M. *Phys. Rev. Lett.* **1990**, *64*, 1039.
(67) Tromp, R. M. *Phys. Rev. B* **1993**, *47*, 7125.
(68) Patthey, L.; Bullock, E. L.; Abukawa, T.; Kono, S.; Johansson, L. S. O. *Phys. Rev. Lett.* **1995**, *75*, 2538.
(69) Qin, X. R. Private communication.
(70) Rudkevich, E.; Liu, F.; Savage, D. S.; McCaugham, L.; Lagally, M. G. *Phys. Rev. Lett.*, submitted for publication.
(71) LeGoues, F. K.; Kean, V. P.; Iyer, S. S.; Tersoff, J.; Tromp, R. M. *Phys. Rev. Lett.* **1990**, *64*, 2038.
(72) Titek, V.; Egami, T. *Phys. Status Solidi (b)* **1987**, *144*, 145.
(73) Kelires, P. C.; Tersoff, J. *Phys. Rev. Lett.* **1989**, *63*, 1164.
(74) Copel, M.; Reuter, M. C.; Horn von Hoegen, M.; Tromp, R. M. *Phys. Rev. B* **1990**, *42*, 11682.
(75) Oyanagi, H.; Sakamoto, K.; Shioda, R.; Sakamoto, T. *Jpn. J. Appl. Phys.* **1994**, *33*, 3545.
(76) Sasaki, M.; Abukawa, T.; Yeom, H. W.; Yamada, M.; Suzuki, S.; Sato, S.; Kono, S. *Appl. Surf. Sci.* **1994**, *82/83*, 387.
(77) Asai, M.; Ueba, H.; Tatsuyama, C. R. *Appl. Phys.* **1985**, *58*, 2577.
(78) Gossman, H. J.; Feldman, L. C.; Gibson, W. M. *Surf. Sci.* **1985**, *155*, 413.
(79) Zinke-Allmang, M.; Feldman, L. C.; Nakahara, S.; Davidson, B. A. *Phys. Rev. B* **1989**, *39*, 7848.
(80) Eaglesham, D. J.; Cerullo, M. *Phys. Rev. Lett.* **1990**, *64*, 1943.
(81) LeGoues, F. K.; Copel, M.; Tromp, R. M. *Phys. Rev. B* **1990**, *42*, 11690.
(82) Tersoff, J. *Phys. Rev. B* **1991**, *43*, 9377.
(83) Lutz, M. A.; Feenstra, R. M.; Mooney, P. M.; Tersoff, J.; Chu, J. O. *Surf. Sci.* **1994,** *316*, L1075.
(84) Chen, K. M.; Jesson, D. E.; Pennycook, S. J.; Mostoller, M.; Kaplan, T.; Thundat, T.; Warmack, R. J. *Phys. Rev. Lett.* **1995**, *75*, 1582.
(85) Vanderbilt, D.; Wickham, L. K. In *Evolution of Thin-Film and Surface Microstructure*; MRS Proceedings Vol. 202, Thompson, C. V., Tsao, J. Y., Srolovitz, D. J., Eds.; Materials Research Society: Pittsburgh, 1991; p 555.
(86) Tersoff, J.; Tromp, R. M. *Phys. Rev. Lett.* **1993**, *70*, 2782.
(87) Tersoff, J.; LeGoues, K. F. *Phys. Rev. Lett.* **1994**, *72*, 3570.
(88) LeGoues, F. K.; Mooney, P. M.; Tersoff, J. *Phys. Rev. Lett.* **1993**, *71*, 396.
(89) Tersoff, J.; Teichert, C.; Lagally, M. G. *Phys. Rev. Lett.* **1996**, *76*, 1675. Teichert, C.; Lagally, M. G.; Peticolas, L. J.; Bean, J. C.; Tersoff, J. *Phys. Rev. B* **1996**, *53*, 16334.
(90) Liu, F.; Lagally, M. G. *Surf. Sci.* **1997**, in press.
(91) Shchukin, V. A.; Ledentsov, N. N.; Kop'ev, P. S.; Bimberg, D. *Phys. Rev. Lett.* **1995**, *75*, 2968.
(92) Steinfort, A. J.; Scholte, P. M. L. O.; Ettema, A.; Tuinstra, F.; Nielsen, M.; Landemark, E.; Smilgies, D. M.; Feidenhans'l, R.; Falkenberg, G.; Seehofer, L.; Johnson, R. L. *Phys. Rev. Lett.*, **1996**, *77*, 2009.
(93) Xie, Y. H.; Gilmer, G. H.; Roland, C.; Silverman, P. J.; Buratto, S. K.; Cheng, J. Y.; Fitzgerald, E. A.; Kortan, A. R.; Schuppler, S.; Marcus, M. A.; Citrin, P. H. *Phys. Rev. Lett.* **1994**, *73*, 1570. Jones, D. E.; Pelz, J. P.; Xie, Y. H.; Silverman, P. J.; Gilmer, G. H. *Phys. Rev. Lett.* **1995**, *75*, 1570.
(94) Phang, Y. H.; Teichert, C.; Lagally, M. G.; Peticolas, T. J.; Bean, J. C.; Kasper, E. *Phys. Rev. B* **1994**, *50*, 14435.
(95) Tersoff, J.; Phang, Y. H.; Zhang, Z. Y.; Lagally, M. G. *Phys. Rev. Lett.* **1995**, *75*, 2730.
(96) Liu, F.; Tersoff, J.; Lagally, M. G. *Phys. Rev. Lett.*, submitted for publication.

CR9600722